IMA Journal of Numerical Analysis (2023) **43**, 663–691
https://doi.org/10.1093/imanum/drab104
Advance Access publication on 23 February 2022

Convergence of Lagrange finite elements for the Maxwell eigenvalue problem in two dimensions

Daniele Boffi
King Abdullah University of Science and Technology, Thuwal 23955-6900, Saudi Arabia, and University of Pavia, Pavia 27100, Italy

Johnny Guzmán*
Division of Applied Mathematics, Brown University, Providence 02912, USA
*Corresponding author: johnny_guzman@brown.edu

and

Michael Neilan
Department of Mathematics, University of Pittsburgh, Pittsburgh 15260, USA

[Received on 16 February 2021; revised on 08 September 2021]

We consider finite element approximations of the Maxwell eigenvalue problem in two dimensions. We prove, in certain settings, convergence of the discrete eigenvalues using Lagrange finite elements. In particular, we prove convergence in three scenarios: piecewise linear elements on Powell–Sabin triangulations, piecewise quadratic elements on Clough–Tocher triangulations and piecewise quartics (and higher) elements on general shape-regular triangulations. We provide numerical experiments that support the theoretical results. The computations also show that, on general triangulations, the eigenvalue approximations are very sensitive to nearly singular vertices, i.e., vertices that fall on exactly two 'almost' straight lines.

Keywords: Maxwell eigenvalues; Lagrange elements.

1. Introduction

Let $\Omega \subset \mathbb{R}^2$ be a contractible polygonal domain and consider the eigenvalue problem: find $\boldsymbol{u} \in \boldsymbol{H}_0(\mathrm{rot}, \Omega)$, $\boldsymbol{u} \neq 0$ and $\eta \in \mathbb{R}$ such that

$$(\mathrm{rot}\,\boldsymbol{u}, \mathrm{rot}\,\boldsymbol{v}) = \eta^2(\boldsymbol{u}, \boldsymbol{v}) \quad \forall\, \boldsymbol{v} \in \boldsymbol{H}_0(\mathrm{rot}, \Omega), \tag{1.1}$$

where $\boldsymbol{H}(\mathrm{rot}, \Omega) := \{\boldsymbol{v} \in \boldsymbol{L}^2(\Omega) : \mathrm{rot}\,\boldsymbol{v} \in L^2(\Omega)\}$, $\boldsymbol{H}_0(\mathrm{rot}, \Omega) := \{\boldsymbol{v} \in \boldsymbol{H}(\mathrm{rot}, \Omega) : \boldsymbol{v} \cdot \boldsymbol{t} = 0 \text{ on } \partial\Omega\}$ and $(\cdot, \cdot)$ denotes the L^2 inner product over Ω. Given a finite element space $\boldsymbol{V}_h \subset \boldsymbol{H}_0(\mathrm{rot}, \Omega)$ a finite element method seeks $\boldsymbol{u}_h \in \boldsymbol{V}_h \backslash \{0\}$ and $\eta_h \in \mathbb{R}$ satisfying

$$(\mathrm{rot}\,\boldsymbol{u}_h, \mathrm{rot}\,\boldsymbol{v}_h) = \eta_h^2(\boldsymbol{u}_h, \boldsymbol{v}_h) \quad \forall\, \boldsymbol{v}_h \in \boldsymbol{V}_h. \tag{1.2}$$

For example, one can take $\boldsymbol{V}_h$ to be the $\boldsymbol{H}_0(\mathrm{rot}; \Omega)$-conforming Nédélec finite elements (i.e., the rotated Raviart–Thomas finite elements) as the finite element space. It is well known this choice leads to a convergent approximation of the eigenvalue problem. On the other hand, taking $\boldsymbol{V}_h$ as a space of continuous piecewise polynomials (i.e., an $\boldsymbol{H}^1(\Omega)$-conforming Lagrange finite element) may lead to spurious eigenvalues for any mesh parameter.

There is a vast literature on this subject. The interested reader is referred to Boffi (2010, Section 20) for an extensive survey including a comprehensive list of references about Nédélec finite elements and to Boffi *et al.* (2000, 1999) for discussion about the use of standard Lagrange finite elements (see also Arnold *et al.*, 2010 for a discussion of these phenomena in the context of the finite element exterior calculus (FEEC)). Many formulations have been developed based on penalization and/or regularization (e.g., Costabel & Dauge, 2002; Buffa *et al.*, 2009; Bonito & Guermond, 2011; Badia & Codina, 2012; Duan *et al.*, 2019a,b; Du & Duan, 2020), showing Lagrange elements can lead to consistent approximations to (1.1). However, we are not aware of a previous analysis of Lagrange elements on macro elements using the standard formulation (1.2), and this is the main objective of this work.

To better appreciate the problem and its discretization we consider the equivalent formulation introduced in Boffi *et al.* (1999) for $\eta \neq 0$: $(\boldsymbol{\sigma}, p) \in \boldsymbol{H}_0(\mathrm{rot}, \Omega) \times L^2_0(\Omega)$, $\boldsymbol{\sigma} \neq 0$ such that

$$(\boldsymbol{\sigma}, \boldsymbol{\tau}) + (p, \mathrm{rot}\, \boldsymbol{\tau}) = 0 \quad \forall\, \boldsymbol{\tau} \in \boldsymbol{H}_0(\mathrm{rot}, \Omega), \tag{1.3a}$$

$$(\mathrm{rot}\, \boldsymbol{\sigma}, q) = -\lambda (p, q) \quad \forall\, q \in L^2_0(\Omega). \tag{1.3b}$$

Taking $q = \mathrm{rot}\, \boldsymbol{v}$ with $\boldsymbol{v} \in \boldsymbol{H}_0(\mathrm{rot}, \Omega)$ shows the equivalence of (1.3) and (1.1) with $\boldsymbol{\sigma} = \boldsymbol{u}, \lambda = \eta^2$ and $p = -\frac{1}{\lambda} \mathrm{rot}\, \boldsymbol{u}$.

The corresponding finite element method for the mixed formulation (1.3) seeks $\boldsymbol{\sigma}_h \in \boldsymbol{V}_h \backslash \{0\}$, $p_h \in Q_h$ and $\lambda_h \in \mathbb{R}$ such that

$$(\boldsymbol{\sigma}_h, \boldsymbol{\tau}_h) + (p_h, \mathrm{rot}\, \boldsymbol{\tau}_h) = 0 \quad \forall\, \boldsymbol{\tau}_h \in \boldsymbol{V}_h, \tag{1.4a}$$

$$(\mathrm{rot}\, \boldsymbol{\sigma}_h, q_h) = -\lambda_h (p_h, q_h) \quad \forall\, q_h \in Q_h, \tag{1.4b}$$

with $Q_h \subset L^2_0(\Omega)$. Similar to the continuous problem, if the finite element spaces satisfy $\mathrm{rot}\, \boldsymbol{V}_h \subset Q_h$, then the mixed finite element formulation (1.4) is equivalent to the primal one (1.2) with $\boldsymbol{\sigma}_h = \boldsymbol{u}_h$, $\lambda_h = \eta_h^2$ and $p_h = -\frac{1}{\lambda_h} \mathrm{rot}\, \boldsymbol{u}_h$.

If $\boldsymbol{V}_h$ is the Nédélec space of index k then we may take Q_h to be the space of piecewise polynomials of degree $k-1$. In this case $(\boldsymbol{V}_h, Q_h)$ forms an inf-sup stable pair of spaces, in particular, there exists a Fortin projection

$$\boldsymbol{\Pi}_V : \boldsymbol{V} \to \boldsymbol{V}_h$$

satisfying

$$\mathrm{rot}\, \boldsymbol{\Pi}_V \boldsymbol{\tau} = \Pi_Q \mathrm{rot}\, \boldsymbol{\tau} \quad \forall\, \boldsymbol{\tau} \in \boldsymbol{V}, \tag{1.5a}$$

$$\|\boldsymbol{\Pi}_V \boldsymbol{\tau} - \boldsymbol{\tau}\|_{L^2(\Omega)} \leqslant C h^{\frac{1}{2}+\delta} (\|\boldsymbol{\tau}\|_{H^{\frac{1}{2}+\delta}(\Omega)} + \|\mathrm{rot}\, \boldsymbol{\tau}\|_{L^2(\Omega)}) \quad \forall\, \boldsymbol{\tau} \in \boldsymbol{V}. \tag{1.5b}$$

Here $\boldsymbol{V} := \boldsymbol{H}_0(\mathrm{rot}, \Omega) \cap \boldsymbol{H}(\mathrm{div}, \Omega)$. Moreover, $\delta \in (0, \frac{1}{2}]$ is a parameter such that $\boldsymbol{V} \hookrightarrow \boldsymbol{H}^{\frac{1}{2}+\delta}(\Omega)$ (Amrouche *et al.*, 1998), and $\Pi_Q : L^2_0(\Omega) \to Q_h$ is the L^2 orthogonal projection onto Q_h. Using this projection one can prove that the corresponding source problems converge uniformly, and this is sufficient to prove convergence of the eigenvalue problem (1.2) (see Boffi, 2010; Kato, 1995 and Proposition 2.1).

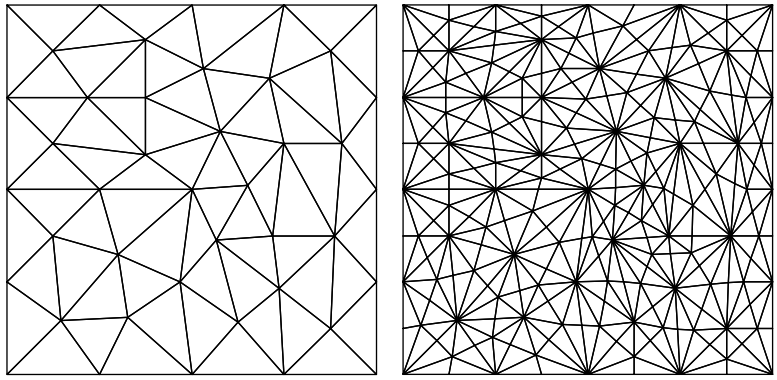

FIG. 1. A simplicial triangulation of the unit square (left) and the associated Powell–Sabin triangulation (right).

On the other hand, if $\boldsymbol{V}_h$ is taken to be the Lagrange finite element space of degree k, then a natural choice of Q_h is the space of (discontinuous) piecewise polynomials of degree $k-1$. However, $(\boldsymbol{V}_h, Q_h)$ is *not* inf-sup stable on generic triangulations, at least when $k=1$ (Qin, 1994; Boffi *et al.*, 2008), and therefore there does not exist a Fortin projection satisfying (1.5). On the other hand, the pair $(\boldsymbol{V}_h, Q_h)$ is known to be stable on special triangulations, even if the inf-sup condition might not be sufficient to guarantee the existence of a Fortin projector satisfying (1.5) (see Boffi *et al.*, 2000).

Wong & Cendes (1988) showed numerically that, on very special triangulations, solutions to (1.2) do converge to the correct eigenvalues using piecewise linear Lagrange elements (i.e., $k=1$). In fact, they used precisely the Powell–Sabin triangulations (see Fig. 1). A rigorous proof of this result has remained unsettled until now; see the review paper Boffi (2010) for a discussion. Specifically, we prove that using Lagrange elements in conjunction with Powell–Sabin triangulation leads to a convergent method. We do this by proving that there is a Fortin projection of sorts. We show that there exists an operator $\boldsymbol{\Pi}_V : \boldsymbol{V}(Q_h) \to \boldsymbol{V}_h$ satisfying

$$\operatorname{rot} \boldsymbol{\Pi}_V \boldsymbol{\tau} = \operatorname{rot} \boldsymbol{\tau} \quad \forall\, \boldsymbol{\tau} \in \boldsymbol{V}(Q_h), \tag{1.6a}$$

$$\|\boldsymbol{\Pi}_V \boldsymbol{\tau} - \boldsymbol{\tau}\|_{L^2(\Omega)} \leqslant C h^{\frac{1}{2}+\delta} (\|\boldsymbol{\tau}\|_{H^{\frac{1}{2}+\delta}(\Omega)} + \|\operatorname{rot} \boldsymbol{\tau}\|_{L^2(\Omega)}) \quad \forall\, \boldsymbol{\tau} \in \boldsymbol{V}(Q_h), \tag{1.6b}$$

where $\boldsymbol{V}(Q_h) = \{\boldsymbol{v} \in \boldsymbol{V} : \operatorname{rot} \boldsymbol{v} \in Q_h\}$. Note that (1.5) implies (1.6), and we prove convergence of the eigenvalue problem whenever there is a projection $\boldsymbol{\Pi}_V$ satisfying (1.6). In addition to linear Lagrange elements on Powell–Sabin triangulations we prove the existence of such a projection on Clough–Tocher splits using quadratic Lagrange elements, and on general triangulations using kth-degree Lagrange elements with $k \geq 4$ (i.e., the Scott–Vogelius finite elements). For the Scott–Vogelius finite elements we find the approximate eigenvalues are extremely sensitive if the mesh has nearly singular vertices, i.e., vertices that fall on exactly two 'almost' straight lines (cf. Section 3.3). We give numerical examples that illustrate this behavior.

The analysis of composite triangulations (e.g., Clough–Tocher and Powell–Sabin) on problem (1.1) goes back at least to the work of Costabel & Dauge (2002). Recently, Duan *et al.* (2019a,b) and Du & Duan (2020) considered Lagrange finite elements for Maxwell's eigenvalue problem in two and three dimensions using composite triangulations. However, as noted earlier, they use a different formulation

from the standard one (1.2). In particular, in Du & Duan (2020) they add a Lagrange multiplier and an equation of the form $(\operatorname{div} \boldsymbol{u}_h, q_h) = 0$ appears, which can be thought of as a Kikuchi-type formulation (Kikuchi, 1989), where one transfers the derivatives to $\boldsymbol{u}_h$. In Duan *et al.* (2019b) a similar formulation is used with a regularization term.

As mentioned above, the main idea to show convergence of Lagrange elements using the standard formulation (1.1) on certain triangulations is the construction of a Fortin-type operation with certain approximation properties. On certain composite triangulations (e.g., Powell–Sabin, Clough–Tocher, Alfeld, Worsey–Farin), exact sequences and/or Fortin projections have been developed; see for example Christiansen & Hu (2018), Fu *et al.* (2020), Guzmán *et al.* (2020a,b), Qin (1994), Zhang (2005). These results have led to stable finite element for fluid flow problems; see for example Neilan (2020). In this paper, for the Powell–Sabin and Clough–Tocher triangulations, we cannot directly use the Fortin projections defined in Fu *et al.* (2020), Guzmán *et al.* (2020a) since they require too much smoothness. Instead, we preprocess with a Scott–Zhang-type interpolant that preserves the vanishing tangential components, and then use the degrees of freedom in Fu *et al.* (2020), Guzmán *et al.* (2020a). These projections are sufficient for our purposes; however, it would be very interesting to see whether one can construct an L^2 bounded commuting projection for these sequences, as is done in the FEEC (Christiansen & Winther, 2008). If bounded L^2 commuting projections exist then the convergence of eigenvalue problems follows from the general theory in FEEC (Arnold *et al.*, 2006, 2010; Boffi, 2010).

The paper is organized as follows: in the next section we give a convergence proof for finite element spaces with stable projections. In Section 3 we provide three examples of Lagrange finite element spaces with stable projections: the piecewise linear Lagrange space on Powell–Sabin splits, the piecewise quadratic Lagrange space on Clough–Tocher splits and the piecewise kth-degree Lagrange space on generic triangulations. In Section 4 we provide numerical experiments and make some concluding remarks in Section 5.

2. Convergence framework

Define the two-dimensional curl , rot, and divergence operators as

$$\operatorname{curl} u = \Big(\frac{\partial u}{\partial x_2}, -\frac{\partial u}{\partial x_1}\Big)^{\mathrm{T}}, \qquad \operatorname{rot} \boldsymbol{v} = \frac{\partial v_2}{\partial x_1} - \frac{\partial v_1}{\partial x_2}, \qquad \operatorname{div} \boldsymbol{v} = \frac{\partial v_1}{\partial x_1} + \frac{\partial v_2}{\partial x_2},$$

and define the Hilbert spaces

$$\begin{aligned} \boldsymbol{H}_0(\operatorname{rot}, \Omega) &= \{\boldsymbol{v} \in \boldsymbol{L}^2(\Omega) : \ \operatorname{rot} \boldsymbol{v} \in L^2(\Omega), \ \boldsymbol{v} \cdot \boldsymbol{t}|_{\partial\Omega} = 0\}, \\ \boldsymbol{H}(\operatorname{div}, \Omega) &= \{\boldsymbol{v} \in \boldsymbol{L}^2(\Omega) : \ \operatorname{div} \boldsymbol{v} \in L^2(\Omega)\}, \\ L^2_0(\Omega) &= \{q \in L^2(\Omega) : \ \textstyle\int_\Omega q = 0\}, \end{aligned}$$

where $\boldsymbol{t}$ is a unit tangent vector of $\partial\Omega$. Recall that $\boldsymbol{V} = \boldsymbol{H}_0(\operatorname{rot}, \Omega) \cap \boldsymbol{H}(\operatorname{div}, \Omega)$.

Let $\boldsymbol{V}_h \subset \boldsymbol{H}_0(\operatorname{rot}, \Omega)$ and $Q_h \subset L^2_0(\Omega)$ be finite element spaces such that $\operatorname{rot} \boldsymbol{V}_h \subset Q_h$.

2.1 *Source problems*

We will require the corresponding source problems for the analysis. To this end we define the solution operators $\boldsymbol{A} : L^2(\Omega) \to \boldsymbol{H}_0(\mathrm{rot}, \Omega)$ and $T : L^2(\Omega) \to L^2_0(\Omega)$ such that for given $f \in L^2(\Omega)$, there holds

$$(\boldsymbol{A}f, \boldsymbol{\tau}) + (Tf, \mathrm{rot}\,\boldsymbol{\tau}) = 0, \quad \forall\, \boldsymbol{\tau} \in \boldsymbol{H}_0(\mathrm{rot}, \Omega), \tag{2.1a}$$

$$(\mathrm{rot}\,\boldsymbol{A}f, q) = (f, q) \quad \forall\, q \in L^2_0(\Omega). \tag{2.1b}$$

Likewise, the discrete source problem is given by the following: find $\boldsymbol{A}_h f \in \boldsymbol{V}_h$ and $T_h f \in Q_h$ such that

$$(\boldsymbol{A}_h f, \boldsymbol{\tau}_h) + (T_h f, \mathrm{rot}\,\boldsymbol{\tau}_h) = 0 \quad \forall\, \boldsymbol{\tau} \in \boldsymbol{V}_h, \tag{2.2a}$$

$$(\mathrm{rot}\,\boldsymbol{A}_h f, q_h) = (f, q_h) \quad \forall\, q_h \in Q_h. \tag{2.2b}$$

Note that $\boldsymbol{A}f = \mathrm{curl}\, Tf$, and so $\mathrm{div}\,\boldsymbol{A}f = 0$. Moreover, using that $\mathrm{rot}\,\boldsymbol{A}f = f$, we have that $\boldsymbol{A}f \in \boldsymbol{V}$.

We define the operator norm:

$$\|T - T_h\| := \sup_{f \in L^2(\Omega)\setminus\{0\}} \frac{\|(T - T_h)f\|_{L^2(\Omega)}}{\|f\|_{L^2(\Omega)}}. \tag{2.3}$$

We will use the next standard result, whicht states that the uniform convergence of the discrete source problem implies convergence of the discrete eigenvalues.

This result is a consequence of the classical discussion in Babuška & Osborn (1991, Section 8) (see also Boffi *et al.*, 1999, Theorem 4.4, and Boffi, 2010, Section 9).

PROPOSITION 2.1 Let T and T_h be defined from (2.1) and (2.2), respectively, and suppose that $\|T - T_h\| \to 0$ as $h \to 0$. Consider problem (1.3) and consider the nonzero eigenvalues $0 < \lambda^{(1)} \leqslant \lambda^{(2)} \leqslant \cdots$. Consider also (1.4) and its nonzero eigenvalues $0 < \lambda_h^{(1)} \leqslant \lambda_h^{(2)} \leqslant \cdots$. Then, for any fixed i, $\lim_{h\to 0} \lambda_h^{(i)} = \lambda^{(i)}$.

Therefore, to prove convergence of eigenvalues it suffices to show uniform convergence of the discrete source problem. To prove this we will exploit the embedding $\boldsymbol{V} \hookrightarrow \boldsymbol{H}^{\frac{1}{2}+\delta}(\Omega)$ along with an assumption on the finite element spaces. The embedding result is proved in three dimensions in Amrouche *et al.* (1998), and we state the two-dimensional version here.

PROPOSITION 2.2 Let Ω be a contractible polygonal domain. Then there exist constants $\delta \in (0, \frac{1}{2}]$ and $C > 0$ such that

$$\|\boldsymbol{v}\|_{H^{\frac{1}{2}+\delta}(\Omega)} \leqslant C(\|\mathrm{div}\,\boldsymbol{v}\|_{L^2(\Omega)} + \|\mathrm{rot}\,\boldsymbol{v}\|_{L^2(\Omega)}) \quad \forall\, \boldsymbol{v} \in \boldsymbol{V}.$$

From now on δ will refer to the delta of the above proposition. We will use the space

$$\boldsymbol{V}(Q_h) = \{\boldsymbol{\tau} \in \boldsymbol{V} : \ \mathrm{rot}\,\boldsymbol{\tau} \in Q_h\}. \tag{2.4}$$

ASSUMPTION 2.3 We assume that $\operatorname{rot} \boldsymbol{V}_h \subset Q_h$ and the existence of a projection $\boldsymbol{\Pi}_V : \boldsymbol{V}(Q_h) \to \boldsymbol{V}_h$ such that

$$\operatorname{rot} \boldsymbol{\Pi}_V \boldsymbol{\tau} = \operatorname{rot} \boldsymbol{\tau} \quad \forall\, \boldsymbol{\tau} \in \boldsymbol{V}(Q_h), \tag{2.5a}$$

$$\|\boldsymbol{\Pi}_V \boldsymbol{\tau} - \boldsymbol{\tau}\|_{L^2(\Omega)} \leqslant \omega_0(h)(\|\boldsymbol{\tau}\|_{H^{\frac{1}{2}+\delta}(\Omega)} + \|\operatorname{rot} \boldsymbol{\tau}\|_{L^2(\Omega)}) \quad \forall\, \boldsymbol{\tau} \in \boldsymbol{V}(Q_h). \tag{2.5b}$$

Furthermore, we assume that the L^2-orthogonal projection $\Pi_Q : L^2(\Omega) \to Q_h$ satisfies

$$\|\Pi_Q \phi - \phi\|_{L^2(\Omega)} \leqslant \omega_1(h) \|\operatorname{curl} \phi\|_{L^2(\Omega)} \qquad \forall\, \phi \in H^1(\Omega) \cap L^2_0(\Omega).$$

Here, the constants are assumed to satisfy $\omega_0(h), \omega_1(h) > 0$, are bounded for $h \in (0, \operatorname{diam}(\Omega)]$ and $\lim_{h \to 0^+} \omega_i(h) = 0$ for $i = 0, 1$.

THEOREM 2.4 Suppose that $(\boldsymbol{V}_h, Q_h)$ satisfy Assumption 2.3. Let T and T_h be defined by (2.1) and (2.2), respectively. Then there holds

$$\|T - T_h\| \leqslant C(\omega_0(h) + \omega_1(h)).$$

Note that Theorem 2.4 and Proposition 2.1 imply that the discrete eigenvalues in the finite element method (1.2) converge to the correct values.

REMARK 2.5 In this paper we focus on the convergence to eigenvalues, but we do not explicitly explore convergence rates. Proving convergence rates requires estimating $T - T_h$ restricted to eigenspaces, so that the regularity of the eigenfunctions can be taken into account (Boffi, 2010, Theorem 9.7).

To prove Theorem 2.4 we require two preliminary results.

LEMMA 2.6 Suppose that Assumption 2.3 is satisfied. Then there exists a constant $C > 0$ such that

$$\|\boldsymbol{A} \Pi_Q f - \boldsymbol{A} f\|_{L^2(\Omega)} + \|T \Pi_Q f - T f\|_{L^2(\Omega)} \leqslant C \omega_1(h) \|f\|_{L^2(\Omega)} \quad \forall f \in L^2(\Omega).$$

Proof. Let $f \in L^2(\Omega)$ and set $\boldsymbol{\sigma} = \boldsymbol{A} f, u = Tf, \boldsymbol{\psi} = \boldsymbol{A} \Pi_Q f$ and $w = T \Pi_Q f$. We see that

$$(\boldsymbol{\sigma} - \boldsymbol{\psi}, \boldsymbol{\tau}) + (u - w, \operatorname{rot} \boldsymbol{\tau}) = 0 \qquad \forall\, \boldsymbol{\tau} \in \boldsymbol{H}_0(\operatorname{rot}, \Omega), \tag{2.6a}$$

$$(\operatorname{rot} (\boldsymbol{\sigma} - \boldsymbol{\psi}), v) = (f - \Pi_Q f, v) \quad \forall\, v \in L^2_0(\Omega). \tag{2.6b}$$

Setting $v = w - u$ in (2.6b) and $\boldsymbol{\tau} = \boldsymbol{\sigma} - \boldsymbol{\psi}$ in (2.6a) and adding the result yields $\|\boldsymbol{\sigma} - \boldsymbol{\psi}\|^2_{L^2(\Omega)} = (f - \Pi_Q f, w - u)$. Furthermore, (2.6a) implies $\operatorname{curl} (u - w) = \boldsymbol{\sigma} - \boldsymbol{\psi}$. Therefore, there holds

$$\|\boldsymbol{\sigma} - \boldsymbol{\psi}\|_{L^2(\Omega)} \leqslant \sup_{\phi \in H^1(\Omega) \cap L^2_0(\Omega)} \frac{(f - \Pi_Q f, \phi)}{\|\operatorname{curl} \phi\|_{L^2(\Omega)}}.$$

However, the properties of the L^2 projection and Assumption 2.3 give us

$$\sup_{\phi\in H^1(\Omega)\cap L^2_0(\Omega)} \frac{(f-\Pi_Q f,\phi)}{\|\operatorname{curl}\phi\|_{L^2(\Omega)}} = \sup_{\phi\in H^1(\Omega)\cap L^2_0(\Omega)} \frac{(f,\phi-\Pi_Q\phi)}{\|\operatorname{curl}\phi\|_{L^2(\Omega)}} \leqslant \omega_1(h)\|f\|_{L^2(\Omega)}.$$

Thus, we have shown

$$\|\boldsymbol{A}\Pi_Q f-\boldsymbol{A}f\|_{L^2(\Omega)} \leqslant \omega_1(h)\|f\|_{L^2(\Omega)}.$$

Finally, because $Tf\in L^2_0(\Omega)$, we have by the Poincaré inequality,

$$\|T\Pi_Q f-Tf\|_{L^2(\Omega)} \leqslant C\|\operatorname{curl}(T\Pi_Q f-Tf)\|_{L^2(\Omega)} = C\|\boldsymbol{A}\Pi_Q f-\boldsymbol{A}f\|_{L^2(\Omega)} \leqslant C\omega_1(h)\|f\|_{L^2(\Omega)}. \quad \square$$

Next we prove that Assumption 2.3 implies the inf-sup condition for the pair $(\boldsymbol{V}_h, Q_h)$.

LEMMA 2.7 Suppose that Assumption 2.3 is satisfied. Then there exists a constant $C>0$ such that for every $u_h\in Q_h$, there exists $\boldsymbol{\tau}_h\in\boldsymbol{V}_h$ such that $\operatorname{rot}\boldsymbol{\tau}_h = u_h$ and $\|\boldsymbol{\tau}_h\|_{L^2(\Omega)} \leqslant C\|u_h\|_{L^2(\Omega)}$.

Proof. From Girault & Raviart (1986, page 81) we have the existence of $\boldsymbol{\tau}\in\boldsymbol{H}^1_0(\Omega)$ with $\operatorname{rot}\boldsymbol{\tau} = u_h$ such that $\|\boldsymbol{\tau}\|_{H^1(\Omega)} \leqslant C\|u_h\|_{L^2(\Omega)}$. Noting that $\boldsymbol{\tau}\in\boldsymbol{V}(Q_h)$, we define $\boldsymbol{\tau}_h = \boldsymbol{\Pi}_V\boldsymbol{\tau}$ so that $\operatorname{rot}\boldsymbol{\tau}_h = \operatorname{rot}\boldsymbol{\tau} = u_h$. Moreover,

$$\|\boldsymbol{\tau}_h\|_{L^2(\Omega)} \leqslant C(\|\boldsymbol{\tau}\|_{H^{\frac{1}{2}+\delta}(\Omega)} + \|\operatorname{rot}\boldsymbol{\tau}\|_{L^2(\Omega)}) \leqslant C\|\boldsymbol{\tau}\|_{H^1(\Omega)} \leqslant C\|u_h\|_{L^2(\Omega)}. \quad \square$$

Now we can prove Theorem 2.4.

Proof of Theorem 2.4. Let $f\in L^2(\Omega)$, and set $\boldsymbol{\sigma} = \boldsymbol{A}f, u = Tf$ and $\boldsymbol{\sigma}_h = \boldsymbol{A}_h f, u_h = T_h f$. Let $\boldsymbol{\psi} = \boldsymbol{A}\Pi_Q f$ and $w = T\Pi_Q f$.

We first derive an estimate for $\boldsymbol{\Pi}_V\boldsymbol{\psi}-\boldsymbol{\sigma}_h$. Using the inclusion $\operatorname{rot}\boldsymbol{V}_h\subset Q_h$ we see that

$$(\boldsymbol{\Pi}_V\boldsymbol{\psi}-\boldsymbol{\sigma}_h,\boldsymbol{\tau}_h) + (\Pi_Q w-u_h,\operatorname{rot}\boldsymbol{\tau}_h) = (\boldsymbol{\Pi}_V\boldsymbol{\psi}-\boldsymbol{\psi},\boldsymbol{\tau}_h) \qquad \forall\,\boldsymbol{\tau}_h\in\boldsymbol{V}_h,$$

$$(\operatorname{rot}(\boldsymbol{\Pi}_V\boldsymbol{\psi}-\boldsymbol{\sigma}_h), v_h) = 0 \qquad \forall\, v_h\in Q_h.$$

Setting $\boldsymbol{\tau}_h = \boldsymbol{\Pi}_V\boldsymbol{\psi}-\boldsymbol{\sigma}_h$ and applying the Cauchy–Schwarz inequality yields

$$\|\boldsymbol{\Pi}_V\boldsymbol{\psi}-\boldsymbol{\sigma}_h\|_{L^2(\Omega)} \leqslant \|\boldsymbol{\Pi}_V\boldsymbol{\psi}-\boldsymbol{\psi}\|_{L^2(\Omega)} \leqslant \omega_0(h)(\|\boldsymbol{\psi}\|_{H^{\frac{1}{2}+\delta}(\Omega)} + \|\operatorname{rot}\boldsymbol{\psi}\|_{L^2(\Omega)}).$$

If we use Proposition 2.2 we get

$$\|\boldsymbol{\psi}\|_{H^{\frac{1}{2}+\delta}(\Omega)} \leqslant C(\|\operatorname{div}\boldsymbol{\psi}\|_{L^2(\Omega)} + \|\operatorname{rot}\boldsymbol{\psi}\|_{L^2(\Omega)}) = C\|\operatorname{rot}\boldsymbol{\psi}\|_{L^2(\Omega)} = C\|\Pi_Q f\|_{L^2(\Omega)} \leqslant C\|f\|_{L^2(\Omega)}.$$

Hence,

$$\|\boldsymbol{\Pi}_V\boldsymbol{\psi} - \boldsymbol{\sigma}_h\|_{L^2(\Omega)} \leqslant C\omega_0(h)\|f\|_{L^2(\Omega)}. \tag{2.7}$$

Using the inf-sup stability stated in Lemma 2.7, Assumption 2.3 and (2.7) we have

$$\|\Pi_Q w - u_h\|_{L^2(\Omega)} \leqslant C\big(\|\boldsymbol{\Pi}_V\boldsymbol{\psi} - \boldsymbol{\psi}\|_{L^2(\Omega)} + \|\boldsymbol{\Pi}_V\boldsymbol{\psi} - \boldsymbol{\sigma}_h\|_{L^2(\Omega)}\big) \leqslant C\omega_0(h)\|f\|_{L^2(\Omega)}.$$

Hence, we have

$$\begin{aligned}\|w - u_h\|_{L^2(\Omega)} &\leqslant C\omega_0(h)\|f\|_{L^2(\Omega)} + \|w - \Pi_Q w\|_{L^2(\Omega)}\\ &\leqslant C\omega_0(h)\|f\|_{L^2(\Omega)} + \omega_1(h)\|\operatorname{curl} w\|_{L^2(\Omega)}.\end{aligned}$$

But we have $\|\operatorname{curl} w\|_{L^2(\Omega)} \leqslant C\|\Pi_Q f\|_{L^2(\Omega)} \leqslant C\|f\|_{L^2(\Omega)}$, and so

$$\|(T - T_h)f\|_{L^2(\Omega)} = \|u - u_h\|_{L^2(\Omega)} \leqslant C(\omega_0(h) + \omega_1(h))\|f\|_{L^2(\Omega)}. \qquad \square$$

REMARK 2.8 Note that by Lemma 2.6,

$$\|\boldsymbol{\sigma} - \boldsymbol{\psi}\|_{L^2(\Omega)} + \|w - u\|_{L^2(\Omega)} \leqslant C\omega_1(h)\|f\|_{L^2(\Omega)},$$

and therefore by (2.7) and Assumption 2.3,

$$\begin{aligned}\|(\boldsymbol{A} - \boldsymbol{A}_h)f\|_{L^2(\Omega)} &= \|\boldsymbol{\sigma} - \boldsymbol{\sigma}_h\|_{L^2(\Omega)}\\ &\leqslant \|\boldsymbol{\sigma} - \boldsymbol{\psi}\|_{L^2(\Omega)} + \|\boldsymbol{\sigma}_h - \boldsymbol{\Pi}_V\boldsymbol{\psi}\|_{L^2(\Omega)} + \|\boldsymbol{\Pi}_V\boldsymbol{\psi} - \boldsymbol{\psi}\|_{L^2(\Omega)}\\ &\leqslant C\omega_0(h)\|f\|_{L^2(\Omega)}.\end{aligned}$$

Thus, we also have $\|\boldsymbol{A} - \boldsymbol{A}_h\| \leqslant C\omega_0(h)$.

3. Examples of Fortin operators

In this section we give examples of finite element pairs satisfying Assumption 2.3, where $\boldsymbol{V}_h$ is taken to be a space of continuous, piecewise polynomials, i.e., a Lagrange finite element space. Here we use recent results on divergence-free finite element pairs for the Stokes problem to construct a Fortin projection satisfying (2.5). A common theme of these Stokes pairs is the imposition of mesh conditions for low-polynomial-degree finite element spaces; it is well known that Assumption 2.3 is not satisfied on general simplicial meshes and for low polynomial degree. Before continuing, we introduce some notation.

We denote by $\mathcal{T}_h$ a shape-regular, simplicial triangulation of Ω with $h_T = \operatorname{diam}(T)$ for all $T \in \mathcal{T}_h$, and $h = \max_{T\in\mathcal{T}_h} h_T$. Let $\mathcal{V}_h^I$, $\mathcal{V}_h^B$, $\mathcal{V}_h^C$ denote the sets of interior vertices, boundary vertices and corner vertices, respectively. Note that the cardinality of $\mathcal{V}_h^C$ is uniformly bounded due to the shape regularity of $\mathcal{T}_h$. The set of all vertices is $\mathcal{V}_h = \mathcal{V}_h^I \cup \mathcal{V}_h^B$. Likewise, $\mathcal{E}_h^I$ and $\mathcal{E}_h^B$ are the sets of interior and boundary

edges, respectively, and $\mathcal{E}_h = \mathcal{E}_h^I \cup \mathcal{E}_h^B$. We denote by $\mathcal{T}_h(z)$ the patch of triangles that have $z \in \mathcal{V}_h$ as a vertex. Likewise, $\mathcal{V}_h^I(T)$ and $\mathcal{V}_h^B(T)$ are the sets of interior and boundary vertices of $T \in \mathcal{T}_h$, and $\mathcal{E}_h^I(T)$ is the set of interior edges of T.

For a non-negative integer k and set $S \subset \Omega$ let $\mathcal{P}_k(S)$ to be the space of piecewise polynomials of degree $\leqslant k$ with domain S. The analogous space of piecewise polynomials with respect to $\mathcal{T}_h$ is

$$\mathcal{P}_k(\mathcal{T}_h) = \prod_{T \in \mathcal{T}_h} \mathcal{P}_k(T),$$

and the Lagrange finite element space is

$$\mathcal{P}_k^c(\mathcal{T}_h) = \mathcal{P}_k(\mathcal{T}_h) \cap H^1(\Omega).$$

Analogous vector-valued spaces are denoted in boldface, e.g., $\mathbf{P}_k(\mathcal{T}_h) = [\mathcal{P}_k(\mathcal{T}_h)]^2$. Finally, the constant C denotes a generic constant that is independent of the mesh parameter h and may take different values at different occurrences.

In the subsequent sections we will employ a Scott–Zhang-type interpolant on the space $\boldsymbol{V}$. We cannot use the Scott–Zhang interpolant directly, as the canonical Scott–Zhang interpolant of a function in $\boldsymbol{V}$ might not have zero tangential components at the corners of Ω; hence, we have to modify the Scott–Zhang interpolant at the corners of Ω. This type of interpolant has been used for example in Bonito & Guermond (2011, (2.14) and (2.15)). For completeness we give a detailed construction in the appendix but we state the result here.

LEMMA 3.1 Let $0 < \delta \leqslant \frac{1}{2}$. There exists a projection $\boldsymbol{I}_h : \boldsymbol{H}^{\frac{1}{2}+\delta}(\Omega) \to \mathbf{P}_1^c(\mathcal{T}_h)$ with the bound

$$h_T^{-\frac{1}{2}-\delta} \|\boldsymbol{\tau} - \boldsymbol{I}_h \boldsymbol{\tau}\|_{L^2(T)} + \|\boldsymbol{I}_h \boldsymbol{\tau}\|_{H^{\frac{1}{2}+\delta}(T)} \leqslant C \|\boldsymbol{\tau}\|_{H^{\frac{1}{2}+\delta}(\omega(T))} \qquad \forall \boldsymbol{\tau} \in \boldsymbol{V}, \tag{3.1}$$

where $\omega(T) = \bigcup_{T' \in \mathcal{T}_h \bar{T} \cap \bar{T}' \neq \emptyset} T'$. Moreover, $\boldsymbol{I}_h \boldsymbol{\tau} \cdot \boldsymbol{t}|_{\partial\Omega} = 0$ if $\boldsymbol{\tau} \cdot \boldsymbol{t}|_{\partial\Omega} = 0$.

3.1 *Construction of a Fortin operator on Powell–Sabin splits*

In this section we use the recent results given in Guzmán *et al.* (2020a) to construct a Fortin projection into the Lagrange finite element space defined on Powell–Sabin triangulations. For simplicity and readability we focus on the lowest-order case; however, the arguments easily extend to arbitrary polynomial degree $k \geq 1$.

Given the simplicial triangulation of $\mathcal{T}_h$ of Ω, we construct its Powell–Sabin refinement $\mathcal{T}_h^{\mathrm{ps}}$ as follows (Guzmán *et al.*, 2020a; Lai & Schumaker, 2007; Powell & Sabin, 1977). First, adjoin the incenter of each $T \in \mathcal{T}_h$ to each vertex of T. Next, the interior points (incenters) of each adjacent pair of triangles are connected with an edge. For any T that shares an edge with the boundary of Ω the midpoint of that edge is connected with the incenter of T. Thus, each $T \in \mathcal{T}_h$ is split into six triangles; cf. Fig. 1.

Let $\mathcal{S}_h^I(\mathcal{T}_h^{\mathrm{ps}})$ be the points of intersection of the interior edges of $\mathcal{T}_h$ that adjoin incenters, let $\mathcal{S}_h^B(\mathcal{T}_h^{\mathrm{ps}})$ be the intersection points of the boundary edges that adjoin incenters and set $\mathcal{S}_h(\mathcal{T}_h^{\mathrm{ps}}) = \mathcal{S}_h^I(\mathcal{T}_h^{\mathrm{ps}}) \cup \mathcal{S}_h^B(\mathcal{T}_h^{\mathrm{ps}})$. Note that, by the definition of the Powell–Sabin split, the points in $\mathcal{S}_h(\mathcal{T}_h^{\mathrm{ps}})$ are the singular vertices in $\mathcal{T}_h^{\mathrm{ps}}$, i.e, the vertices that lie on exactly two straight lines. In particular, for a vertex $z \in \mathcal{S}_h^I(\mathcal{T}_h^{\mathrm{ps}})$ there exist four triangles $\mathcal{T}_h^{\mathrm{ps}}(z) = \{T_i\}_{i=1}^4 \subset \mathcal{T}_h^{\mathrm{ps}}$ such that z is a vertex of T_i. Without loss of generality

we assume that these triangles are labeled in a counterclockwise direction. We then define for a scalar function v,

$$\theta_z(v) := v|_{T_1}(z) - v|_{T_2}(z) + v|_{T_3}(z) - v|_{T_4}(z). \tag{3.2}$$

We then define the spaces

$$\boldsymbol{V}_h = \mathbf{P}_1^c(\mathcal{T}_h^{\mathrm{ps}}) \cap \boldsymbol{H}_0(\mathrm{rot}, \Omega), \tag{3.3a}$$

$$Q_h = \{v \in \mathcal{P}_0(\mathcal{T}_h^{\mathrm{ps}}) \cap L_0^2(\Omega) : \ \theta_z(v) = 0 \ \forall z \in \mathcal{S}_h^I(\mathcal{T}_h^{\mathrm{ps}})\}. \tag{3.3b}$$

LEMMA 3.2 (Guzmán *et al.* (2020a)). Let $\boldsymbol{V}_h$ and Q_h be defined by (3.3). Then there holds $\mathrm{rot}\, \boldsymbol{V}_h \subset Q_h$.

We now extend the results of Guzmán *et al.* (2020a) to construct an appropriate Fortin operator that is well defined for $\boldsymbol{\tau} \in \boldsymbol{V}(Q_h)$. To do so we require some additional notation.

For an interior singular vertex $z \in \mathcal{S}_h(\mathcal{T}_h^{\mathrm{ps}})$ let $T \in \mathcal{T}_h$ be a triangle in $\mathcal{T}_h$ such that $z \in \partial T$, and let $\{K_1, K_2\} \subset \mathcal{T}_h^{\mathrm{ps}}$ be the triangles in $\mathcal{T}_h^{\mathrm{ps}}$ such that $K_1, K_2 \subset T$ and $K_1, K_2 \in \mathcal{T}_h^{\mathrm{ps}}(z)$. Let $e = \partial K_1 \cap \partial K_2$, and let $\mathbf{m}_i$ be the outward unit normal of K_i perpendicular to e. We then define the jump of a scalar piecewise smooth function at z (restricted to T) as

$$[\![v]\!]_T(z) = v\big|_{K_1}(z)\mathbf{m}_1 + v\big|_{K_2}(z)\mathbf{m}_2.$$

Note that $[\![v]\!]_T(z)$ is single valued for all $v \in Q_h$. In particular, if z is an interior singular vertex with $z \in \partial T_1 \cap \partial T_2$ for some $T_1, T_2 \in \mathcal{T}_h$, $T_1 \neq T_2$, then $[\![v]\!]_{T_1}(z) = [\![v]\!]_{T_2}(z)$ for all $v \in Q_h$ because $\theta_z(v) = 0$. Therefore, we shall omit the subscript and simply write $[\![v]\!](z)$.

Next, for a triangle $T \in \mathcal{T}_h$ in the nonrefined mesh, we denote by T^{ct} the resulting set of three triangles obtained by connecting the barycenter of T to its vertices, i.e., T^{ct} is the Clough–Tocher refinement of T. We define the set of (local) piecewise polynomials with respect to this partition as

$$\mathcal{P}_k(T^{\mathrm{ct}}) = \prod_{K \in T^{\mathrm{ct}}} \mathcal{P}_k(K). \tag{3.4}$$

The following lemma provides the degrees of freedom for $\boldsymbol{V}_h$ and Q_h that will be used to construct the Fortin operator. The result essentially follows from Guzmán *et al.* (2020a, Lemmas 10–11).

LEMMA 3.3 A function $\boldsymbol{\tau} \in \boldsymbol{V}_h$ is uniquely defined by the conditions

$$\boldsymbol{\tau}(z) \qquad \forall z \in \mathcal{V}_h^I, \tag{3.5a}$$

$$\boldsymbol{\tau}(z) \cdot \boldsymbol{n} \qquad \forall z \in \mathcal{V}_h^B \backslash \mathcal{V}_h^C, \tag{3.5b}$$

$$\int_e (\boldsymbol{\tau} \cdot \boldsymbol{t}) \qquad \forall e \in \mathcal{E}_h^I, \tag{3.5c}$$

$$[\![\mathrm{rot}\, \boldsymbol{\tau}]\!](z) \qquad \forall z \in \mathcal{S}_h(\mathcal{T}_h^{\mathrm{ps}}), \tag{3.5d}$$

$$\int_T (\operatorname{rot}\boldsymbol{\tau})r \qquad \forall\, r \in \mathcal{P}_0(T^{\mathrm{ct}}) \cap L_0^2(T),\ \forall\, T \in \mathcal{T}_h. \tag{3.5e}$$

Moreover, a function $v \in Q_h$ is uniquely determined by the values

$$[\![v]\!](z) \qquad \forall\, z \in \mathcal{S}_h(\mathcal{T}_h^{\mathrm{ps}}), \tag{3.6a}$$

$$\int_T vr \qquad \forall\, r \in \mathcal{P}_0(T^{\mathrm{ct}}),\ \forall\, T \in \mathcal{T}_h. \tag{3.6b}$$

THEOREM 3.4 Let $\boldsymbol{V}_h$ and Q_h be defined by (3.3), and let $\boldsymbol{V}(Q_h)$ be defined by (2.4). Then there exists a projection $\boldsymbol{\Pi}_V : \boldsymbol{V}(Q_h) \to \boldsymbol{V}_h$ such that $\operatorname{rot}\boldsymbol{\Pi}_V\boldsymbol{p} = \operatorname{rot}\boldsymbol{p}$ for all $\boldsymbol{p} \in \boldsymbol{V}(Q_h)$. Moreover,

$$\|\boldsymbol{\tau} - \boldsymbol{\Pi}_V\boldsymbol{\tau}\|_{L^2(\Omega)} \leqslant C\big(h^{\frac{1}{2}+\delta}\|\boldsymbol{\tau}\|_{H^{\frac{1}{2}+\delta}(\Omega)} + h\|\operatorname{rot}\boldsymbol{\tau}\|_{L^2(\Omega)}\big) \qquad \forall\, \boldsymbol{\tau} \in \boldsymbol{V}(Q_h).$$

Proof. Fix $\boldsymbol{\tau} \in \boldsymbol{V}(Q_h)$, and let $\boldsymbol{I}_h\boldsymbol{\tau} \in \mathbf{P}_1^c(\mathcal{T}_h) \cap \boldsymbol{H}_0(\operatorname{rot}, \Omega) \subset \boldsymbol{V}_h$ be the modified Scott–Zhang interpolant of $\boldsymbol{\tau}$ established in Lemma 3.1. We then construct $\boldsymbol{\Pi}_V\boldsymbol{\tau}$ via the conditions

$$(\boldsymbol{\Pi}_V\boldsymbol{\tau})(z) = (\boldsymbol{I}_h\boldsymbol{\tau})(z) \qquad \forall\, z \in \mathcal{V}_h^I, \tag{3.7a}$$

$$(\boldsymbol{\Pi}_V\boldsymbol{\tau})(z)\cdot\boldsymbol{n} = (\boldsymbol{I}_h\boldsymbol{\tau})(z)\cdot\boldsymbol{n} \qquad \forall\, z \in \mathcal{V}_h^B\backslash\mathcal{V}_h^C, \tag{3.7b}$$

$$\int_e (\boldsymbol{\Pi}_V\boldsymbol{\tau})\cdot\boldsymbol{t} = \int_e \boldsymbol{\tau}\cdot\boldsymbol{t} \qquad \forall\, e \in \mathcal{E}_h^I, \tag{3.7c}$$

$$\big[\!\big[\operatorname{rot}\boldsymbol{\Pi}_V\boldsymbol{\tau}\big]\!\big](z) = [\![\operatorname{rot}\boldsymbol{\tau}]\!](z) \qquad \forall\, z \in \mathcal{S}_h(\mathcal{T}_h^{\mathrm{ps}}), \tag{3.7d}$$

$$\int_T (\operatorname{rot}\boldsymbol{\Pi}_V\boldsymbol{\tau})r = \int_T (\operatorname{rot}\boldsymbol{\tau})r \qquad \forall\, r \in \mathcal{P}_0(T^{\mathrm{ct}}) \cap L_0^2(T),\ \forall\, T \in \mathcal{T}_h. \tag{3.7e}$$

The arguments given in Guzmán *et al.* (2020a) show that $\operatorname{rot}\boldsymbol{\Pi}_V\boldsymbol{\tau} = \operatorname{rot}\boldsymbol{\tau}$,

By scaling, there holds for each $\boldsymbol{\sigma}_h \in \boldsymbol{V}_h$ and on each $T \in \mathcal{T}_h$,

$$\begin{aligned}\|\boldsymbol{\sigma}_h\|_{L^2(T)}^2 \leqslant C\Big[h_T^2\Big(&\sum_{z\in\mathcal{V}_h^I(T)} |\boldsymbol{\sigma}_h(z)|^2 + \sum_{z\in\mathcal{V}_h^B(T)\backslash\mathcal{V}_h^C(T)} |\boldsymbol{\sigma}_h(z)\cdot\boldsymbol{n}|^2\Big)\\ &+ \sum_{e\in\mathcal{E}_h^I(T)} \Big|\int_e \boldsymbol{\sigma}_h\cdot\boldsymbol{t}\Big|^2 + h_T^2 \sup_{\substack{r\in\mathcal{P}_0(T^{\mathrm{ct}})\\ \|r\|_{L^2(T)}=1}} \Big|\int_T (\operatorname{rot}\boldsymbol{\sigma}_h)r\Big|^2\\ &+ h_T^4 \sum_{z\in\mathcal{S}_h(T)} \big|\big[\!\big[\operatorname{rot}\boldsymbol{\sigma}_h\big]\!\big](z)\big|^2\Big],\end{aligned}$$

where $\mathcal{S}_h(T)$ is the set of singular vertices contained in $\bar{T}$. Now set $\boldsymbol{\sigma}_h = \boldsymbol{\Pi}_V\boldsymbol{\tau} - \boldsymbol{I}_h\boldsymbol{\tau}$. Using the above estimate and (3.7) then yields

$$\|\boldsymbol{\Pi}_V\boldsymbol{\tau} - \boldsymbol{I}_h\boldsymbol{\tau}\|^2_{L^2(T)} \leqslant C\Big[\Big|\int_{\partial T}(\boldsymbol{\tau} - \boldsymbol{I}_h\boldsymbol{\tau})\cdot\boldsymbol{t}\Big|^2 + h_T^2 \sup_{\substack{r\in\mathcal{P}_0(T^{\mathrm{ct}})\\ \|r\|_{L^2(T)}=1}} \Big|\int_T \mathrm{rot}\,(\boldsymbol{\tau} - \boldsymbol{I}_h\boldsymbol{\tau})r\Big|^2 + h_T^4 \sum_{z\in\mathcal{S}_h(T)} \big|\big[\!\big[\mathrm{rot}\,(\boldsymbol{\tau} - \boldsymbol{I}_h\boldsymbol{\tau})\big]\!\big](z)\big|^2\Big]. \tag{3.8}$$

Because $\mathrm{rot}\,(\boldsymbol{\tau} - \boldsymbol{I}_h\boldsymbol{\tau}) \in Q_h$ we use the degrees of freedom (3.6) and a scaling argument to conclude that

$$\sup_{\substack{r\in\mathcal{P}_0(T^{\mathrm{ct}})\\ \|r\|_{L^2(T)}=1}} \Big|\int_T (\mathrm{rot}\,(\boldsymbol{\tau} - \boldsymbol{I}_h\boldsymbol{\tau})r\Big|^2 + h_T^2 \sum_{z\in\mathcal{S}_h(T)} \big|\big[\!\big[\mathrm{rot}\,(\boldsymbol{\tau} - \boldsymbol{I}_h\boldsymbol{\tau})\big]\!\big](z)\big|^2 \leqslant C\|\mathrm{rot}\,(\boldsymbol{\tau} - \boldsymbol{I}_h\boldsymbol{\tau})\|^2_{L^2(T)}. \tag{3.9}$$

We then use an inverse estimate to get

$$\begin{aligned}\|\mathrm{rot}\,(\boldsymbol{\tau} - \boldsymbol{I}_h\boldsymbol{\tau})\|^2_{L^2(T)} &\leqslant C\big[\|\mathrm{rot}\,\boldsymbol{\tau}\|^2_{L^2(T)} + \|\nabla\boldsymbol{I}_h\boldsymbol{\tau}\|^2_{L^2(T)}\big]\\ &\leqslant C\big[\|\mathrm{rot}\,\boldsymbol{\tau}\|^2_{L^2(T)} + h_T^{-1+2\delta}\|\boldsymbol{I}_h\boldsymbol{\tau}\|^2_{H^{\frac12+\delta}(T)}\big].\end{aligned} \tag{3.10}$$

Applying estimates (3.9)–(3.10) to (3.8) we obtain

$$\begin{aligned}\|\boldsymbol{\Pi}_V\boldsymbol{\tau} - \boldsymbol{I}_h\boldsymbol{\tau}\|^2_{L^2(T)} &\leqslant C\Big[\Big|\int_{\partial T}(\boldsymbol{\tau} - \boldsymbol{I}_h\boldsymbol{\tau})\cdot\boldsymbol{t}\Big|^2 + h_T^2\big(\|\mathrm{rot}\,\boldsymbol{\tau}\|^2_{L^2(T)} + h_T^{-1+2\delta}\|\boldsymbol{I}_h\boldsymbol{\tau}\|^2_{H^{\frac12+\delta}(T)}\big)\Big]\\ &\leqslant C\big[h_T\|\boldsymbol{\tau} - \boldsymbol{I}_h\boldsymbol{\tau}\|^2_{L^2(\partial T)} + h_T^{1+2\delta}\|\boldsymbol{I}_h\boldsymbol{\tau}\|^2_{H^{\frac12+\delta}(T)} + h_T^2\|\mathrm{rot}\,\boldsymbol{\tau}\|^2_{L^2(T)}\big].\end{aligned}$$

A trace inequality yields (cf. Ern & Guermond, 2017, Lemma 7.2)

$$h_T\|\boldsymbol{\tau} - \boldsymbol{I}_h\boldsymbol{\tau}\|^2_{L^2(\partial T)} \leqslant C\big[\|\boldsymbol{\tau} - \boldsymbol{I}_h\boldsymbol{\tau}\|^2_{L^2(T)} + h_T^{1+2\delta}\|\boldsymbol{\tau} - \boldsymbol{I}_h\boldsymbol{\tau}\|^2_{H^{\frac12+\delta}(T)}\big],$$

and therefore

$$\|\boldsymbol{\Pi}_V\boldsymbol{\tau} - \boldsymbol{I}_h\boldsymbol{\tau}\|^2_{L^2(T)} \leqslant C\big[\|\boldsymbol{\tau} - \boldsymbol{I}_h\boldsymbol{\tau}\|^2_{L^2(T)} + h_T^{1+2\delta}\|\boldsymbol{I}_h\boldsymbol{\tau}\|^2_{H^{\frac12+\delta}(T)} + h_T^{1+2\delta}\|\boldsymbol{\tau}\|^2_{H^{\frac12+\delta}(T)} + h_T^2\|\mathrm{rot}\,\boldsymbol{\tau}\|^2_{L^2(T)}\big].$$

We then apply (3.1) and sum over $T \in \mathcal{T}_h$ to obtain

$$\|\boldsymbol{\Pi}_V\boldsymbol{\tau} - \boldsymbol{I}_h\boldsymbol{\tau}\|_{L^2(\Omega)} \leqslant C\big[h^{\frac12+\delta}\|\boldsymbol{\tau}\|_{H^{\frac12+\delta}(\Omega)} + h\|\mathrm{rot}\,\boldsymbol{\tau}\|_{L^2(\Omega)}\big].$$

Therefore

$$\begin{aligned}\|\boldsymbol{\tau}-\boldsymbol{\Pi}_V\boldsymbol{\tau}\|_{L^2(\Omega)} &\leqslant \|\boldsymbol{\tau}-\boldsymbol{I}_h\boldsymbol{\tau}\|_{L^2(\Omega)}+\|\boldsymbol{\Pi}_V\boldsymbol{\tau}-\boldsymbol{I}_h\boldsymbol{\tau}\|_{L^2(\Omega)}\\ &\leqslant C\big[h^{\frac{1}{2}+\delta}\|\boldsymbol{\tau}\|_{H^{\frac{1}{2}+\delta}(\Omega)}+h\|\operatorname{rot}\boldsymbol{\tau}\|_{L^2(\Omega)}\big].\end{aligned}$$ □

3.2 *Construction of a Fortin operator on Clough–Tocher splits*

The Clough–Tocher refinement of $\mathcal{T}_h$ is obtained by connecting the barycenter of each $T\in\mathcal{T}_h$ with its vertices; thus, each triangle is split into three triangles. In this section we show that there exists a Fortin projection mapping onto the Lagrange finite element space satisfying Assumption 2.3. This result holds for all polynomial degrees $k\geq 2$ but, for simplicity, we only consider the lowest-order case $k=2$.

Let $\mathcal{T}_h^{\mathrm{ct}}$ be the resulting Clough–Tocher refinement of $\mathcal{T}_h$, and define the spaces

$$\boldsymbol{V}_h=\mathbf{P}_2^c(\mathcal{T}_h^{\mathrm{ct}})\cap\boldsymbol{H}_0(\operatorname{rot},\Omega),\tag{3.11a}$$

$$Q_h=L_0^2(\Omega)\cap\mathcal{P}_1(\mathcal{T}_h^{\mathrm{ct}}).\tag{3.11b}$$

It is well known that $\operatorname{rot}\boldsymbol{V}_h\subset Q_h$ (Fu *et al.*, 2020).

Below we modify the results in Fu *et al.* (2020) to build a Fortin projection that is well defined on $\boldsymbol{H}^{\frac{1}{2}+\delta}(\Omega)$ and has optimal-order convergence properties in $\boldsymbol{L}^2(\Omega)$. To this end we first provide a useful set of degrees of freedom for $\boldsymbol{V}_h$ (Fu *et al.*, 2020).

LEMMA 3.5 A function $\boldsymbol{\tau}\in\boldsymbol{V}_h$ is uniquely determined by the values

$$\boldsymbol{\tau}(z)\qquad\forall\, z\in\mathcal{V}_h^I,\tag{3.12}$$

$$\boldsymbol{\tau}(z)\cdot\boldsymbol{n}\qquad\forall\, z\in\mathcal{V}_h^B\backslash\mathcal{V}_h^C,\tag{3.13}$$

$$\int_e\boldsymbol{\tau}\qquad\forall\, e\in\mathcal{E}_h^I,\tag{3.14}$$

$$\int_e\boldsymbol{\tau}\cdot\boldsymbol{n}\qquad\forall\, e\in\mathcal{E}_h^B,\tag{3.15}$$

$$\int_T(\operatorname{rot}\boldsymbol{\tau})r\qquad\forall\, r\in\mathcal{P}_1(T^{\mathrm{ct}})\cap L_0^2(T),\ \forall\, T\in\mathcal{T}_h,\tag{3.16}$$

where $\mathcal{P}_1(T^{\mathrm{ct}})$ is defined by (3.4).

THEOREM 3.6 Let $\boldsymbol{V}_h$ and Q_h be defined by (3.11), and let Π_Q be the L^2 projection onto Q_h. Then there exists a projection $\boldsymbol{\Pi}_V:\boldsymbol{V}(Q_h)\to\boldsymbol{V}_h$, such that $\operatorname{rot}\boldsymbol{\Pi}_V\boldsymbol{\tau}=\Pi_Q(\operatorname{rot}\boldsymbol{\tau})$, Moreover,

$$\|\boldsymbol{\tau}-\boldsymbol{\Pi}_V\boldsymbol{\tau}\|_{L^2(\Omega)}\leqslant C\big(h^{\frac{1}{2}+\delta}\|\boldsymbol{\tau}\|_{H^{\frac{1}{2}+\delta}(\Omega)}+h\|\operatorname{rot}\boldsymbol{\tau}\|_{L^2(\Omega)}\big)\quad\forall\,\boldsymbol{\tau}\in\boldsymbol{V}_h.$$

Proof. Define $\boldsymbol{\Pi}_V$ uniquely by the conditions

$$(\boldsymbol{\Pi}_V\boldsymbol{\tau})(z) = (\boldsymbol{I}_h\boldsymbol{\tau})(z) \qquad \forall\, z \in \mathcal{V}_h^I, \tag{3.17a}$$

$$(\boldsymbol{\Pi}_V\boldsymbol{\tau})(z)\cdot\boldsymbol{n} = (\boldsymbol{I}_h\boldsymbol{\tau})(z)\cdot\boldsymbol{n} \qquad \forall\, z \in \mathcal{V}_h^B\backslash\mathcal{V}_h^C, \tag{3.17b}$$

$$\int_e (\boldsymbol{\Pi}_V\boldsymbol{\tau}) = \int_e \boldsymbol{\tau} \qquad \forall\, e \in \mathcal{E}_h^I, \tag{3.17c}$$

$$\int_e (\boldsymbol{\Pi}_V\boldsymbol{\tau}\cdot\boldsymbol{n}) = \int_e \boldsymbol{\tau}\cdot\boldsymbol{n} \qquad \forall\, e \in \mathcal{E}_h^B, \tag{3.17d}$$

$$\int_T (\operatorname{rot}\boldsymbol{\Pi}_V\boldsymbol{\tau})r = \int_T (\operatorname{rot}\boldsymbol{\tau})r \qquad \forall\, r \in \mathcal{P}_1(T^{\mathrm{ct}}) \cap L_0^2(T),\ \forall\, T \in \mathcal{T}_h. \tag{3.17e}$$

The arguments given in Fu *et al.* (2020) show that $\operatorname{rot}\boldsymbol{\Pi}_V\boldsymbol{\tau} = \Pi_Q\operatorname{rot}\boldsymbol{\tau}$. The same scaling arguments given in Theorem 3.4 show that $\|\boldsymbol{\tau} - \boldsymbol{\Pi}_V\boldsymbol{\tau}\|_{L^2(\Omega)} \leqslant C\big(h^{\frac{1}{2}+\delta}\|\boldsymbol{\tau}\|_{H^{\frac{1}{2}+\delta}(\Omega)} + h\|\operatorname{rot}\boldsymbol{\tau}\|_{L^2(\Omega)}\big)$. □

3.3 *Construction of a Fortin operator on general triangulations*

In this section we construct a Fortin operator for the original Scott–Vogelius pair developed in Scott & Vogelius (1985). This pair essentially takes the space $\boldsymbol{V}_h$ to be the Lagrange space of degree $k \geq 4$, and Q_h to be the space of piecewise polynomials of degree $(k-1)$. As pointed out in Scott & Vogelius (1985) the exact definition of these spaces and their stability is mesh dependent and depends on the presence of singular or 'nearly singular' vertices.

Recall that a singular vertex is a vertex in $\mathcal{T}_h$ that lies on exactly two straight lines. To make this precise, for a vertex $z \in \mathcal{V}_h$, we enumerate the triangles that have z as a vertex as $\mathcal{T}_h(z) = \{T_1, T_2, \ldots, T_N\}$. If z is a boundary vertex then we enumerate the triangles such that T_1 and T_N have a boundary edge. Moreover, we enumerate them so that T_j, T_{j+1} share an edge for $j = 1, \ldots, N-1$ and T_N and T_1 share an edge in the case z is an interior vertex. Let θ_j denote the angle between the edges of T_j originating from z. We define

$$\Theta(z) = \begin{cases} \max\{|\sin(\theta_1+\theta_2)|, \ldots, |\sin(\theta_{N-1}+\theta_N)|, |\sin(\theta_N+\theta_1)|\} & \text{if } z \in \mathcal{V}_h^I, \\ \max\{|\sin(\theta_1+\theta_2)|, \ldots, |\sin(\theta_{N-1}+\theta_N)|\} & \text{if } z \in \mathcal{V}_h^B \text{ and } N \geq 2, \\ 0 & \text{if } z \in \mathcal{V}_h^B \text{ and } N = 1. \end{cases} \tag{3.18}$$

Definition 3.7 A vertex $z \in \mathcal{V}_h$ is a singular vertex if $\Theta(z) = 0$. It is nonsingular if $\Theta(z) > 0$.

We denote all the singular vertices by

$$\mathcal{S}_h = \{z \in \mathcal{V}_h :\ \Theta(z) = 0\}.$$

We further let $\mathcal{S}_h^I$ denote the set of interior singular vertices, $\mathcal{S}_h^B$ the set of boundary singular vertices and $\mathcal{S}_h^C$ the set of corner singular vertices. Equivalently,

$$\mathcal{S}_h^I = \{z \in \mathcal{S}_h : \ \#\mathcal{T}_h(z) = 4\},$$
$$\mathcal{S}_h^B = \{z \in \mathcal{S}_h : \ \#\mathcal{T}_h(z) \in \{1, 2\}\},$$
$$\mathcal{S}_h^C = \{z \in \mathcal{S}_h : \ \#\mathcal{T}_h(z) = 1\}.$$

DEFINITION 3.8 We set

$$\Theta_{\min} := \min_{z \in \mathcal{V}_h \setminus \mathcal{S}_h} \Theta(z). \tag{3.19}$$

For a non-negative integer k we define the spaces

$$\boldsymbol{V}_h = \mathbf{P}_k^c(\mathcal{T}_h) \cap \boldsymbol{H}_0(\mathrm{rot}, \Omega), \tag{3.20a}$$

$$Q_h = \{v \in L_0^2(\Omega) \cap \mathcal{P}_{k-1}(\mathcal{T}_h) : \ \theta_z(v) = 0 \ \forall z \in \mathcal{S}_h^I, \ v(z) = 0 \ \forall z \in \mathcal{S}_h^C\}, \tag{3.20b}$$

where we recall that $\theta_z(v)$ is defined by (3.2).

First we note that the rot operator maps $\boldsymbol{V}_h$ into Q_h (Scott & Vogelius, 1985).

LEMMA 3.9 There holds $\mathrm{rot}\, \boldsymbol{\tau} \in Q_h$ for all $\boldsymbol{\tau} \in \boldsymbol{V}_h$.

Let $\boldsymbol{I}_h$ be Scott–Zhang interpolant onto $\mathbf{P}_1^c(\mathcal{T}_h) \cap \boldsymbol{H}_0(\mathrm{rot}; \Omega) \subset \boldsymbol{V}_h$. Then define $\boldsymbol{I}_1 : \boldsymbol{H}^{\frac{1}{2}+\delta}(\Omega) \to \boldsymbol{V}_h$ as follows:

$$\begin{aligned}
\boldsymbol{I}_1 \boldsymbol{\tau}(z) &= \boldsymbol{I}_h \boldsymbol{\tau}(z) \qquad \forall z \in \mathcal{V}_h, \\
\int_e \boldsymbol{I}_1 \boldsymbol{\tau} \cdot \boldsymbol{\psi} &= \int_e \boldsymbol{\tau} \cdot \boldsymbol{\psi} \qquad \text{for all } \boldsymbol{\psi} \in \mathbf{P}_{k-2}(e), \ \forall e \in \mathcal{E}_h, \\
\int_T \boldsymbol{I}_1 \boldsymbol{\tau} \cdot \boldsymbol{\psi} &= \int_T \boldsymbol{\tau} \cdot \boldsymbol{\psi} \qquad \text{for all } \boldsymbol{\psi} \in \mathbf{P}_{k-3}(T), \ \forall T \in \mathcal{T}_h.
\end{aligned}$$

Standard arguments yield the following result.

LEMMA 3.10 There holds for all $\boldsymbol{\tau} \in \boldsymbol{H}^{\frac{1}{2}+\delta}(\Omega)$,

$$\|\boldsymbol{\tau} - \boldsymbol{I}_1 \boldsymbol{\tau}\|_{L^2(\Omega)} \leqslant C h^{\frac{1}{2}+\delta} \|\boldsymbol{\tau}\|_{H^{\frac{1}{2}+\delta}(\Omega)} \tag{3.21}$$

and

$$\|\mathrm{rot}(\boldsymbol{I}_1 \boldsymbol{\tau})\|_{L^2(\Omega)} \leqslant h^{-\frac{1}{2}+\delta} \|\boldsymbol{\tau}\|_{H^{\frac{1}{2}+\delta}(\Omega)}. \tag{3.22}$$

Moreover, for $k \geq 2$,

$$\int_T \operatorname{rot} \boldsymbol{I}_1 \boldsymbol{\tau} = \int_T \operatorname{rot} \boldsymbol{\tau} \quad \forall\, T \in \mathcal{T}_h. \tag{3.23}$$

The following result follows from Guzmán & Scott (2019, Lemma 6).

LEMMA 3.11 Suppose that $k \geq 4$. Then there exists an injective linear operator $\boldsymbol{J}_1 : Q_h \to \boldsymbol{V}_h$ such that

$$\operatorname{rot}(\boldsymbol{J}_1 v)(z) = v(z) \quad \forall\, z \in \mathcal{V}_h, \tag{3.24a}$$

$$\int_T \operatorname{rot}(\boldsymbol{J}_1 v)\, \mathrm{d}x = 0 \quad \forall\, T \in \mathcal{T}_h, \tag{3.24b}$$

$$\|\boldsymbol{J}_1 v\|_{L^2(\Omega)} + h\|\nabla \boldsymbol{J}_1 v\|_{L^2(\Omega)} \leqslant Ch\Big(\frac{1}{\Theta_{\min}} + 1\Big)\|v\|_{L^2(\Omega)}. \tag{3.24c}$$

The next result follows from Falk & Neilan (2013), Guzmán & Scott (2019), Scott & Vogelius (1985).

LEMMA 3.12 Define

$$\mathcal{Q}_h = \{v \in Q_h : \int_T v = 0\ \forall\, T \in \mathcal{T}_h, \text{ and } v(z) = 0\ \forall\, z \in \mathcal{V}_h\}.$$

Then there exists an injective operator $\boldsymbol{J}_2 : \mathcal{Q}_h \to \boldsymbol{V}_h$ such that

$$\operatorname{rot}(\boldsymbol{J}_2 v) = v,$$
$$\|\boldsymbol{J}_2 v\|_{L^2(\Omega)} + h\|\nabla \boldsymbol{J}_2 v\|_{L^2(\Omega)} \leqslant Ch\|v\|_{L^2(\Omega)}.$$

THEOREM 3.13 Let $\boldsymbol{V}_h$ and Q_h be defined by (3.20) with $k \geq 4$. Then there exists a projection $\boldsymbol{\Pi}_V : \boldsymbol{V}(Q_h) \to \boldsymbol{V}_h$ such that

$$\operatorname{rot}(\boldsymbol{\Pi}_V \boldsymbol{\tau}) = \operatorname{rot} \boldsymbol{\tau}$$

with the following bound

$$\|\boldsymbol{\tau} - \boldsymbol{\Pi}_V \boldsymbol{\tau}\|_{L^2(\Omega)} \leqslant C\big(1 + \Theta_{\min}^{-1}\big)h^{\frac{1}{2}+\delta}\|\boldsymbol{\tau}\|_{H^{\frac{1}{2}+\delta}(\Omega)}.$$

Proof. Define

$$\boldsymbol{\Pi}_V \boldsymbol{\tau} = \boldsymbol{I}_1 \boldsymbol{\tau} + \boldsymbol{J}_1 v_1 + \boldsymbol{J}_2 v_2 \in \boldsymbol{V}_h,$$

where

$$v_1 = \operatorname{rot}(\boldsymbol{\tau} - \boldsymbol{I}_1 \boldsymbol{\tau}) \in Q_h, \qquad v_2 = v_1 - \operatorname{rot}(\boldsymbol{J}_1 v_1) \in Q_h.$$

By Lemma 3.11 and the definition of v_2 we see that

$$v_2(z) = 0 \qquad \forall z \in \mathcal{V}_h,$$

and

$$\int_T v_2 = \int_T \big(v_1 - \operatorname{rot}(\boldsymbol{J}_1 v_1)\big) = \int_T v_1 = \int_T \operatorname{rot}(\boldsymbol{\tau} - \boldsymbol{I}_1\boldsymbol{\tau}) = 0$$

by Lemma 3.10. Therefore $v_2 \in \mathcal{Q}_h$, and so $\boldsymbol{J}_2 v_2$ is well defined (cf. Lemma 3.12).

We then use Lemma 3.12 to get

$$\begin{aligned}
\operatorname{rot}(\boldsymbol{\Pi}_V\boldsymbol{\tau}) &= \operatorname{rot}(\boldsymbol{I}_1\boldsymbol{\tau}) + \operatorname{rot}(\boldsymbol{J}_1 v_1) + \operatorname{rot}(\boldsymbol{J}_2 v_2)\\
&= \operatorname{rot}(\boldsymbol{I}_1\boldsymbol{\tau}) + \operatorname{rot}(\boldsymbol{J}_1 v_1) + v_2\\
&= \operatorname{rot}(\boldsymbol{I}_1\boldsymbol{\tau}) + \operatorname{rot}(\boldsymbol{J}_1 v_1) + (v_1 - \operatorname{rot}(\boldsymbol{J}_1 v_1))\\
&= \operatorname{rot}(\boldsymbol{I}_1\boldsymbol{\tau}) + v_1\\
&= \operatorname{rot}(\boldsymbol{I}_1\boldsymbol{\tau}) + \operatorname{rot}(\boldsymbol{\tau} - \boldsymbol{I}_1\boldsymbol{\tau})\\
&= \operatorname{rot}\boldsymbol{\tau}.
\end{aligned}$$

Now we note that, by (3.22),

$$\begin{aligned}
\|\operatorname{rot}(\boldsymbol{\tau} - \boldsymbol{I}_1\boldsymbol{\tau})\|_{L^2(\Omega)} &\leqslant \|\operatorname{rot}\boldsymbol{\tau}\|_{L^2(\Omega)} + \|\operatorname{rot}(\boldsymbol{I}_1\boldsymbol{\tau})\|_{L^2(\Omega)}\\
&\leqslant \|\operatorname{rot}\boldsymbol{\tau}\|_{L^2(\Omega)} + h^{-\frac{1}{2}+\delta}\|\boldsymbol{\tau}\|_{H^{\frac{1}{2}+\delta}(\Omega)}. \qquad (3.25)
\end{aligned}$$

Next, by Lemma 3.11 and (3.25), we obtain

$$\begin{aligned}
\|\boldsymbol{J}_1 v_1\|_{L^2(\Omega)} &\leqslant Ch\Big(\frac{1}{\Theta_{\min}} + 1\Big)\|v_1\|_{L^2(\Omega)} \qquad (3.26)\\
&\leqslant Ch\Big(\frac{1}{\Theta_{\min}} + 1\Big)\|\operatorname{rot}(\boldsymbol{\tau} - \boldsymbol{I}_1\boldsymbol{\tau})\|_{L^2(\Omega)}\\
&\leqslant C\Big(\frac{1}{\Theta_{\min}} + 1\Big)(h\|\operatorname{rot}\boldsymbol{\tau}\|_{L^2(\Omega)} + h^{\frac{1}{2}+\delta}\|\boldsymbol{\tau}\|_{H^{\frac{1}{2}+\delta}(\Omega)}).
\end{aligned}$$

Likewise, we use Lemmas 3.12 and (3.25) to obtain

$$\begin{aligned}\|\boldsymbol{J}_2 v_2\|_{L^2(\Omega)} &\leqslant Ch\|v_2\|_{L^2(\Omega)} \\ &\leqslant Ch\big(\|v_1\|_{L^2(\Omega)} + \|\mathrm{rot}(\boldsymbol{J}_1 v_1)\|_{L^2(\Omega)}\big) \\ &\leqslant C\big(h\|\mathrm{rot}(\boldsymbol{\tau} - \boldsymbol{I}_1\boldsymbol{\tau})\|_{L^2(\Omega)} + \|\boldsymbol{J}_1 v_1\|_{L^2(\Omega)}\big) \\ &\leqslant C\Big(\frac{1}{\Theta_{\min}} + 1\Big)(h\|\mathrm{rot}\,\boldsymbol{\tau}\|_{L^2(\Omega)} + h^{\frac{1}{2}+\delta}\|\boldsymbol{\tau}\|_{H^{\frac{1}{2}+\delta}(\Omega)}).\end{aligned} \tag{3.27}$$

We then use the triangle inequality, Lemma 3.10, (3.26) and (3.27) to obtain the L^2 error estimate:

$$\begin{aligned}\|\boldsymbol{\tau} - \boldsymbol{\Pi}_V\boldsymbol{\tau}\|_{L^2(\Omega)} &\leqslant \|\boldsymbol{\tau} - \boldsymbol{I}_1\boldsymbol{\tau}\|_{L^2(\Omega)} + \|\boldsymbol{J}_1 v_1\|_{L^2(\Omega)} + \|\boldsymbol{J}_2 v_2\|_{L^2(\Omega)} \\ &\leqslant C\Big(\frac{1}{\Theta_{\min}} + 1\Big)h^{\frac{1}{2}+\delta}\|\boldsymbol{\tau}\|_{H^{\frac{1}{2}+\delta}(\Omega)}.\end{aligned}$$

Finally, if $\boldsymbol{\tau} \in \boldsymbol{V}_h$, then $\boldsymbol{I}_1\boldsymbol{\tau} = \boldsymbol{\tau}$ and so $v_1 = 0$. It then follows that $\boldsymbol{J}_1 v_1 = 0$, and $\boldsymbol{J}_2 v_2 = -\boldsymbol{J}_2(\mathrm{rot}(\boldsymbol{J}_1 v_1)) = 0$. Therefore $\boldsymbol{\Pi}_V\boldsymbol{\tau} = \boldsymbol{I}_1\boldsymbol{\tau} = \boldsymbol{\tau}$, i.e., $\boldsymbol{\Pi}_V$ is a projection. □

4. Numerical experiments

In this section we confirm the theoretical results with some numerical experiments on a variety of meshes and finite element spaces. All the numerical experiments were performed using FEniCS (Alnaes *et al.*, 2015). In the first four tests we take the domain to be the unit square $\Omega = (0,1)^2$. The exact eigenvectors, corresponding to nonzero eigenvalues, are $\boldsymbol{u}^{(n,m)}(x,y) := \mathrm{curl}\, p^{(n,m)}$ where $p^{(n,m)} := \cos(\pi nx)\cos(\pi my)$, with eigenvalues $\lambda^{(n,m)} := \pi^2(n^2+m^2)$ for $n,m \in \mathbb{N}\cup\{0\}$ and $nm \neq 0$. In the following we relabel the nonzero eigenvalues $\lambda^{(i)}$ in nondecreasing order: $0 < \lambda^{(1)} \leqslant \lambda^{(2)} \leqslant \lambda^{(3)} \leqslant \cdots$.

4.1 *Linear Lagrange elements on Powell–Sabin triangulations*

In these series of tests we compute the finite element method (1.2) using piecewise linear Lagrange elements defined on Powell–Sabin triangulations. We create a sequence of generic Delaunay triangulations $\mathcal{T}_h$ with mesh size $h_j = 2^{-j}$ for $j = 3,4,5,6$, and perform the refinement algorithm described in Section 3.1 to obtain a Powell–Sabin triangulation $\mathcal{T}_h^{\mathrm{ps}}$ for each mesh parameter.

In Table 1 we show the first 10 nonzero approximate eigenvalues and errors using method (1.2) defined on $\mathcal{T}_h^{\mathrm{ps}}$ for fixed $h = 1/32$. In Table 2 we list the rate of convergence of the first eigenvalue with respect to h. The tables show an absence of spurious eigenvalues, which agrees with the theoretical results, Theorems 2.4 and 3.4. In addition, we observe an asymptotic quadratic rate of convergence for the computed eigenvalue.

4.2 *Quadratic Lagrange elements on Clough–Tocher triangulations*

In this section we compute the finite element method (1.2) using quadratic Lagrange elements defined on Clough–Tocher triangulations (cf. Section 3.2). As before we create a sequence of meshes $\mathcal{T}_h$ with $h_j = 2^{-j}$ ($j = 3,4,5,6$), and construct the Clough–Tocher refinement $\mathcal{T}_h^{\mathrm{ct}}$ by connecting the vertices of each triangle in $\mathcal{T}_h$ with its barycenter; see Fig. 2.

TABLE 1 *Approximate eigenvalues of (1.2) using the piecewise linear Lagrange finite element space on a Powell–Sabin triangulation. The mesh parameter is* $h = 2^{-5}$

i	$\lambda_h^{(i)}$	$\lvert\lambda^{(i)} - \lambda_h^{(i)}\rvert$
1	9.872556542826	2.952141736802360E−3
2	9.872647617226	3.043216136799032E−3
3	19.75126057536	1.205177318315975E−2
4	39.52514303832	4.672543396706175E−2
5	39.52979992791	5.138232355238159E−2
6	49.42354393173	7.552192628650545E−2
7	49.43033089264	8.230888719544538E−2
8	79.15457141878	1.977362100693938E−1
9	89.06160447391	2.351648641029839E−1
10	89.07453060702	2.480909972125715E−1

TABLE 2 *The rate of convergence with respect to h of the first nonzero eigenvalue using the Powell–Sabin split and the linear Lagrange finite element space*

h	$\lvert\lambda^{(1)} - \lambda_h^{(1)}\rvert$	Rate
2^{-3}	1.084194558097806E−1	
2^{-4}	3.835460507298371E−2	1.8228
2^{-5}	2.952141736802360E−3	1.8768
2^{-6}	7.488421347368046E−4	1.9790

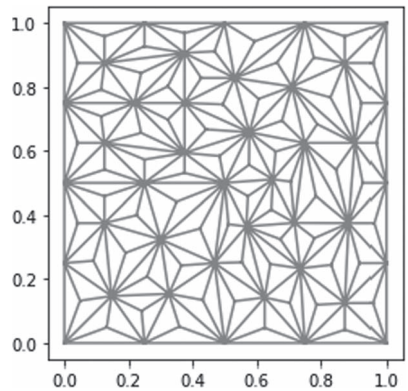

FIG. 2. A Clough–Tocher triangulation with $h = 2^{-3}$.

In Table 3 we report the first computed 10 nonzero approximate eigenvalues using method (1.2). As predicted by Theorems 2.4 and 3.6 the results show accurate approximations with no spurious eigenvalues. In Table 4 we list the rate of convergence to the first eigenvalue for different values of h. The table shows an asymptotic quartic rate of convergence: $\lvert\lambda^{(1)} - \lambda_h^{(1)}\rvert = \mathcal{O}(h^4)$.

TABLE 3 *Approximate eigenvalues using quadratic Lagrange elements on a Clough–Tocher triangulation with* $h = 2^{-5}$

i	$\lambda_h^{(i)}$	$\lvert\lambda^{(i)} - \lambda_h^{(i)}\rvert$
1	9.869606458779	2.057689641788E−6
2	9.869606625899	2.224809986018E−6
3	19.73922733515	1.853298115861E−5
4	39.47853970719	1.221028349079E−4
5	39.47855143244	1.338280896661E−4
6	49.34827341503	2.514095869017E−4
7	49.34829772352	2.757180775106E−4
8	78.95794423573	1.109027018615E−3
9	88.82788915584	1.449546038714E−3
10	88.82798471962	1.545109821734E−3

TABLE 4 *The rate of convergence of the first nonzero eigenvalue using the Clough–Tocher split and* $k = 2$

h	$\lvert\lambda^{(1)} - \lambda_h^{(1)}\rvert$	Rate
2^{-3}	2.98012061403341E−4	
2^{-4}	2.96722579697928E−5	3.3282
2^{-5}	2.05768964178787E−6	3.8500
2^{-6}	1.43249797801559E−7	3.8444

4.3 *Quartic Lagrange elements on criss-cross triangulations*

In this section we compute the finite element method (1.2) using fourth-degree Lagrange elements on several types of triangulations. Theorems 2.4 and 3.13 indicate that this scheme leads to convergent eigenvalue approximations as $h \to 0$ if the quantity $\Theta_{\min}$ is uniformly bounded from below. We recall that the quantity $\Theta_{\min}$ gives a measurement of the closest-to-singular vertex in the mesh, i.e., $\Theta_{\min}$ is small if there exists a vertex in $\mathcal{T}_h$ that falls on two 'almost' straight lines; see (3.19) and (3.18) for the precise definition.

In the first series of tests we numerically study the effect of $\Theta_{\min}$ in finite element method (1.2). To this end we first take $\mathcal{T}_h$ to be the criss-cross mesh with $h = 1/6$ (cf. Fig. 3). This triangulation has 36 singular vertices, but $\Theta_{\min}$ is well behaved. Theorems 2.4 and 3.13 indicate that finite element scheme (1.2) (with quartic Lagrange elements) leads to accurate approximations. Indeed, Table 5 lists the first 10 computed nonzero eigenvalues, and it clearly shows accurate results.

Next we perform the same tests but randomly perturb each singular vertex of the criss-cross mesh by a factor αh for some $\alpha \in (0, 1]$. In particular, for each singular vertex $z \in \mathcal{S}_h$ of the criss-cross triangulation $\mathcal{T}_h$, we make the perturbation $z \to z + (\pm\alpha h, \pm\alpha h)$. Figures 3(right), 4(left) and 4(right) show the resulting triangulations with $\alpha = 0.01$, $\alpha = 0.05$ and $\alpha = 0.1$, respectively. We note that on the resulting perturbed mesh, $\Theta_{\min} \approx \alpha$, and therefore Theorem 3.13 suggests that the finite element approximation (1.2) may suffer for small α-values.

The computed eigenvalues, with values $\alpha = 0.01$, $\alpha = 0.05$ and $\alpha = 0.1$, are reported in Tables 6, 7 and 8, respectively. Table 8 shows that, for relatively large perturbations ($\alpha = 0.1$), we compute

TABLE 5 *Approximate eigenvalues using quartic Lagrange elements on a criss-cross mesh with* $h = 1/6$

i	$\lambda_h^{(i)}$	$\lvert\lambda^{(i)} - \lambda_h^{(i)}\rvert$
1	9.869604401309	2.199112003609E−10
2	9.869604401309	2.200408744102E−10
3	19.73920880459	2.414715538634E−09
4	39.47841782951	2.251546860066E−07
5	39.47841782951	2.251547499554E−07
6	49.34802238840	3.829525141441E−07
7	49.34802238840	3.829534165334E−07
8	78.95683762620	2.417486058448E−06
9	88.82645223886	1.262905662713E−05
10	88.82645223886	1.262905958299E−05

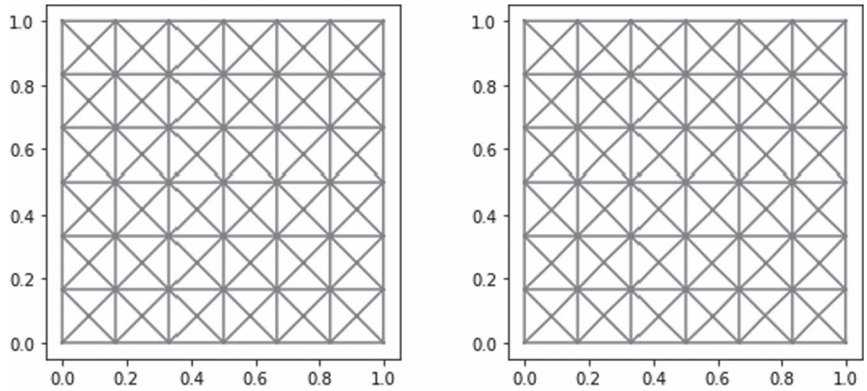

FIG. 3. Left: criss-cross mesh with $h = 1/6$. Right: the mesh obtained by randomly perturbing the singular vertices of the criss-cross mesh by $0.01h$.

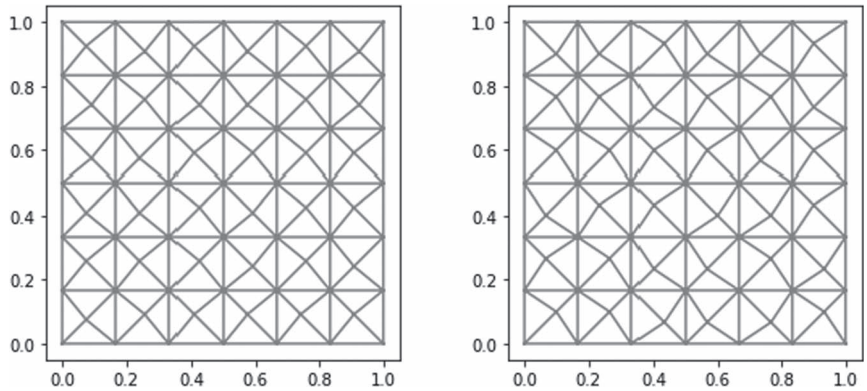

FIG. 4. Criss-cross meshes with singular vertices randomly perturbed by $0.05h$ (left) and $0.1h$ (right).

TABLE 6 *Approximate eigenvalues using quartic Lagrange elements on a* $0.01h$*-perturbed criss-cross mesh with* $h = 1/6$.

i	$\lambda_h^{(i)}$	$\lvert\lambda^{(i)} - \lambda_h^{(i)}\rvert$
1	1.424154538647	8.445449862442
2	1.471404605901	8.398199795188
3	1.477776343297	18.26143245888
4	1.502342236815	37.97607536754
5	1.526468793982	37.95194881038
6	1.540736126805	47.80728587864
7	1.552154885100	47.79586712035
8	1.556952619119	77.39988258960
9	1.566640464185	87.25979914562
10	1.580713040988	87.24572656882

TABLE 7 *Approximate eigenvalues using quartic Lagrange elements on a* $0.05h$*-perturbed criss-cross mesh with* $h = 1/6$

i	$\lambda_h^{(i)}$	$\lvert\lambda^{(i)} - \lambda_h^{(i)}\rvert$
1	9.869604401311	2.212932059820E−10
2	9.869604401311	2.215134742301E−10
3	19.73920880479	2.614239491550E−09
4	35.63498774612	3.843429858239
5	36.48359498561	2.994822618752
6	36.92351459416	12.42450741128
7	37.63299206644	11.71502993900
8	37.78514981304	41.17168539568
9	38.10084364520	50.72559596460
10	38.35191236801	50.47452724179

relatively accurate eigenvalue approximations with similar convergence properties found on the criss-cross mesh (cf. Table 5). On the other hand, for smaller perturbations ($\alpha = 0.05$ and $\alpha = 0.01$), the results drastically differ. Table 6 clearly shows extremely poor approximations for all eigenvalues, and Table 7 only computes the first few eigenvalues with reasonable accuracy before the results deteriorate. These numerical tests indicate the approximation properties of the computed eigenvalues are highly sensitive to the quantity $\Theta_{\min}$.

4.4 *Quartic Lagrange elements on generic triangulations*

Our next series of tests compute finite element method (1.2) using quartic Lagrange elements on generic Delaunay triangulations. Again, Theorem 3.13 and the previous set of tests indicate the approximation properties of the computed eigenvalues are highly sensitive to the quantity $\Theta_{\min}$. In light of this, for a given (generic) triangulation $\mathcal{T}_h$, we randomly move each interior vertex with four neighboring triangles by a $0.1h$-perturbation; see Fig. 5.

TABLE 8 *Approximate eigenvalues using quartic Lagrange elements on a* $0.1h$*-perturbed criss-cross mesh with* $h = 1/6$

i	$\lambda_h^{(i)}$	$\lvert\lambda^{(i)} - \lambda_h^{(i)}\rvert$
1	9.869604401320	2.310134306071E−10
2	9.869604401320	2.312834368468E−10
3	19.73920880546	3.285371974471E−09
4	39.47841784038	2.360199999885E−07
5	39.47841784071	2.363495781310E−07
6	49.34802242662	4.211773898533E−07
7	49.34802246288	4.574410894520E−07
8	78.95683842488	3.216167357323E−06
9	88.82645270371	1.309390694360E−05
10	88.82645276747	1.315766178323E−05

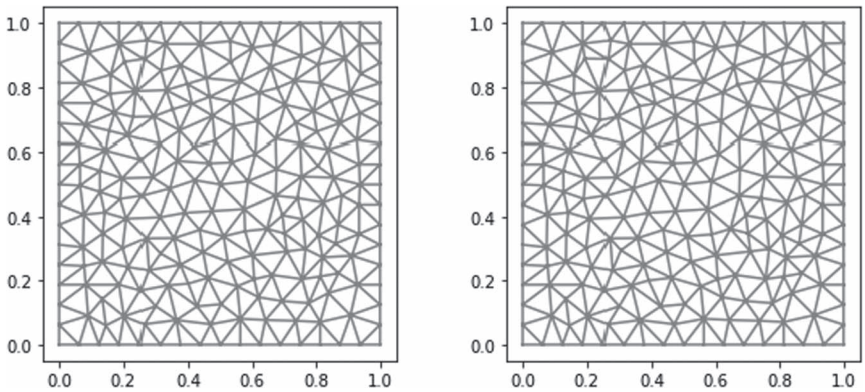

FIG. 5. (left) Unstructured mesh with $h \approx 1/10$, (right) randomly perturbing interior vertices who have four triangles by at most $0.1h$.

TABLE 9 *Maximum error of the first* 20 *eigenvalues on perturbed Delaunay triangulations using quartic Lagrange elements*

h	$\max_{1\leqslant i\leqslant 20} \lvert\lambda^{(i)} - \lambda_h^{(i)}\rvert$	Rate
2^{-2}	8.3861134511E−03	
2^{-3}	5.6183112093E−05	7.2217
2^{-4}	2.2360291041E−07	7.9731
2^{-5}	8.9832496997E−10	7.9595

Table 9 shows the maximum errors of the first 20 computed eigenvalues on these perturbed meshes for $h = 2^{-j}$ $(j = 2, 3, 4, 5)$. The table clearly shows convergence with rate $\mathcal{O}(h^8)$. On the other hand, the errors of the computed eigenvalues on 'non-perturbed' meshes do not converge, as shown in Table 10.

TABLE 10 *Maximum error of the first* 20 *eigenvalues on (nonperturbed) Delaunay triangulations using quartic Lagrange elements. Note that for* $h = 2^{-2}$ *and* $h = 2^{-3}$*, the mesh* $\mathcal{T}_h$ *does not have any vertices with four neighboring triangles*

h	$\max_{1\leqslant i\leqslant 20} \lvert\lambda^{(i)} - \lambda_h^{(i)}\rvert$	Rate
2^{-2}	8.38611345105E−03	
2^{-3}	5.61831120933E−05	7.2217
2^{-4}	59.2176263988	−20.008
2^{-5}	59.2176264065	0.000

TABLE 11 *L-shaped domain: the rate of convergence of the first nonzero eigenvalue using the Powell–Sabin split and* $k = 1$

h	$\lvert\lambda^{(1)} - \lambda_h^{(1)}\rvert$	Rate
2^{-3}	5.29957E−03	
2^{-4}	2.42718E−03	1.12659499
2^{-5}	1.07087E−03	1.18049541
2^{-6}	5.5788E−04	0.94076660
2^{-7}	1.8099E−04	1.62402935
2^{-8}	7.273E−05	1.31537097

It is interesting to note that Costabel & Dauge (2002) showed that using quartics one has convergence on any mesh if the stabilization term (div, div) is added to the formulation (at least for convex polygons). However, here we see that the results are more sensitive with formulation (1.1).

4.5 *L-shaped domains*

In this example we consider an L-shaped domain: $\Omega = [-\pi,\pi]^2\backslash\big([0,\pi]\times[-\pi,0]\big)$. The first nonzero eigenvalue corresponds to an eigenvector that is not in H^1 and the approximate value of this eigenvalue is given by $\lambda^{(1)} \approx 0.149511749824251$ (Dauge, 2003). In Table 11 we give the error using Lagrange elements with $k = 1$ on Powell–Sabin splits. In Table 12 we give the error using Nédélec elements of the second kind with $k = 1$ on the same meshes. As we can see, the rate of convergence seems to be tending to 4/3 for both finite elements, although the errors using the Nédélec elements give more accurate approximations. However, the Nédélec space has significantly more degrees of freedom than the linear Lagrange finite element space. The next eigenvalues correspond to eigenvectors that belong to H^1 and the convergence rates increase to 2 for both elements, but we do not present the errors here.

We would like to stress that although the eigenvalues do converge as we proved, the convergence of the eigenvectors will not converge in $H(\mathrm{div})\cap H(\mathrm{curl})$ if the eigenfunctions are not in H^1. Instead convergence should be sought in the $H(\mathrm{curl})$ norm.

TABLE 12 *L-shaped domain: the rate of convergence of the first nonzero eigenvalue using the Nédélec elements of the second kind and* $k = 1$

h	$\lvert\lambda^{(1)} - \lambda_h^{(1)}\rvert$	Rate
2^{-3}	9.564E−05	
2^{-4}	6.285E−05	0.60567278
2^{-5}	3.039E−05	1.04839118
2^{-6}	1.763E−05	0.78534429
2^{-7}	5.72E−06	1.62460510
2^{-8}	2.41E−06	1.24527844

5. Concluding remarks

In this paper we studied and numerically verified the use of Lagrange finite element spaces for the two-dimensional Maxwell eigenvalue problem. Using and extending the analysis of divergence-free Stokes pairs we showed, on certain triangulations, convergence of the discrete eigenvalues.

While the focus of this paper has been on the two-dimensional setting, the tools developed here may apply to three dimensions as well. In particular, smooth, discrete de Rham complexes using Lagrange finite element spaces have been constructed in Fu *et al.* (2020), Guzmán *et al.* (2020b), and these results might be applicable to the three-dimensional Maxwell eigenvalue problem.

Acknowledgements

D.B. is member of INdAM Research group GNCS and his research is partially supported by PRIN/MIUR and IMATI/CNR.

REFERENCES

ALNAES, M. S., BLECHTA, J., HAKE, J., JOHANSSON, A., KEHLET, B., LOGG, A., RICHARDSON, C., RING, J., ROGNES, M. E. & WELLS, G. N. (2015) The FEniCS Project Version 1.5. *Archive of Numerical Software*, vol. 3.

AMROUCHE, C., BERNARDI, C., DAUGE, M. & GIRAULT, V. (1998) Vector potentials in three-dimensional non-smooth domains. *Math. Meth. Appl. Sci.*, **21**, 823–864.

ARNOLD, D. N., FALK, R. S. & WINTHER, R. (2006) Finite element exterior calculus, homological techniques, and applications. *Acta Numer.*, **15**, 1–55.

ARNOLD, D. N., R. S. FALK, & R. WINTHER (2010) Finite element exterior calculus: from Hodge theory to numerical stability. *Bull. Amer. Math. Soc. (N.S.)*, **47**, 281–354.

BABUŠKA, I. & OSBORN, J. (1991) *Finite Element Methods (Part 1)*. North–Holland, Amsterdam.

BADIA, S. & R. CODINA (2012) A nodal-based finite element approximation of the Maxwell problem suitable for singular solutions. *SIAM J. Numer. Anal.*, **50**, 398–417.

BELLIDO, J. C. & C. MORA-CORRAL (2014) Existence for nonlocal variational problems in peridynamics. *SIAM J. Math. Anal.*, **46**, 890–916.

BOFFI, D. (2010) Finite element approximation of eigenvalue problems. *Acta Numer.*, **19**, 1–120.

BOFFI, D., BREZZI, F., DEMKOWICZ, L., DURÁN, R. G., FALK, R. S. & FORTIN, M. (2008) *Mixed Finite Elements, Compatibility Conditions, and Applications*. Lectures given at the C.I.M.E. Summer School held in Cetraro, Italy June 26–July 1, 2006. Berlin; Fondazione C.I.M.E., Florence: Springer.

Boffi, D., F. Brezzi & L. Gastaldi (2000) On the problem of spurious eigenvalues in the approximation of linear elliptic problems in mixed form. *Math. Comp.*, **69**, 121–140.

Boffi, D., P. Fernandes, L. Gastaldi & I. Perugia (1999) Computational models of electromagnetic resonators: analysis of edge element approximation. *SIAM J. Numer. Anal.*, **36**, 1264–1290.

Bonito, A. & J.-L. Guermond (2011) Approximation of the eigenvalue problem for the time harmonic Maxwell system by continuous Lagrange finite elements. *Math. Comp.*, **80**, 1887–1910.

Buffa, A., P. Ciarlet Jr. & E. Jamelot (2009) Solving electromagnetic eigenvalue problems in polyhedral domains with nodal finite elements. *Numer. Math.*, **113**, 497–518.

Christiansen, S. H. & K. Hu (2018) Generalized finite element systems for smooth differential forms and Stokes' problem. *Numer. Math.*, **140**, 327–71.

Christiansen, S. & R. Winther (2008) Smoothed projections in finite element exterior calculus. *Math. Comp.*, **77**, 813–829.

Ciarlet, P. (2013) Analysis of the Scott–Zhang interpolation in the fractional order Sobolev spaces. *J. Numer. Math.*, **21**, 173–180.

Costabel, M. & M. Dauge (2002) Weighted regularization of Maxwell equations in polyhedral domains. A rehabilitation of nodal finite elements. *Numer. Math.*, **93**, 239–277.

Dauge, M. (2003) Benchmark computations for Maxwell equations for the approximation of highly singular solutions. Available at https://perso.univ-rennes1.fr/monique.dauge/benchmax.html.

Drelichman, I. & R. G. Durán (2018) Improved Poincaré inequalities in fractional Sobolev spaces. *Ann. Acad. Sci. Fennicæ. Math.*, **43**, 885–903.

Du, Z. & H. Duan (2020) A mixed method for Maxwell eigenproblem. *J. Sci. Comput.* **82**, paper no. 8, 37pp.

Duan, H., Z. Du, W. Liu & S. Zhang (2019a) New mixed elements for Maxwell equations. *SIAM J. Numer. Anal.*, **57**, 320–54.

Duan, H., Liu, W., Ma, J., Tan, R. C. E. & Zhang, S. (2019b) A family of optimal Lagrange elements for Maxwell's equations. *J. Comput. Appl. Math.*, **358**, 241–265.

Ern, A. & J.-L. Guermond (2017) Finite element quasi-interpolation and best approximation. *ESAIM: M2AN*, **51**, 1367–85.

Falk, R. & M. Neilan (2013) Stokes complexes and the construction of stable finite elements with pointwise mass conservation. *SIAM J. Numer. Anal.*, **51**, 1308–1326.

Fu, G., J. Guzmán, & M. Neilan (2020) Exact smooth piecewise polynomial sequences on Alfeld splits. *Math. Comp.*, **89**, 1059–1091.

Girault, V. & Raviart, P.-A. (1986) *Finite Element Methods for Navier–Stokes Equations*. Berlin: Springer.

Guzmán, J., A. Lischke & M. Neilan (2020a) Exact sequences on Powell–Sabin splits. *Calcolo*, **57**, 1–25.

Guzmán, J., A. Lischke & M. Neilan (2020b) Exact sequences on Worsey–Farin splits. arXiv:2008.05431.

Guzmán, J. & R. Scott (2019) The Scott–Vogelius finite elements revisited. *Math. Comp.*, **88**, 515–529.

Kato, T. (1995) *Perturbation Theory for Linear Operators*. Reprint of the 1980 edition. Classics in Mathematics. Berlin: Springer.

Kikuchi, F. (1989) On a discrete compactness property for the Nédélec finite elements. *J. Faculty of Science, U. Tokyo. Sect. 1 A, Math.*, **36**, 479–490.

Lai, M.-J. & Schumaker, L. L. (2007) *Spline Functions on Triangulations*. Cambridge: Cambridge University Press.

Neilan, M. (2020) The Stokes complex: A review of exactly divergence–free finite element pairs for incompressible flows. *75 Years of Mathematics of Computation: Symposium on Celebrating 75 Years of Mathematics of Computation, November 1-3, 2018, the Institute for Computational and Experimental Research in Mathematics (ICERM)*. Contemporary Mathematics, vol. 754. American Mathematical Soc., p. 141.

Powell, M. J. D. & M. A. Sabin (1977) Piecewise quadratic approximations on triangles. *Assoc. Comput. Mach. Trans. Math. Softw.* **3**, 316–325.

Qin, J. (1994) On the convergence of some low order mixed finite elements for incompressible fluids. *Ph.D. Thesis*, The Pennsylvania State University.

Scott, L. R. & M. Vogelius (1985) Norm estimates for a maximal right inverse of the divergence operator in spaces of piecewise polynomials. *ESAIM: M2AN* **19**, 111–143.
Scott, L. R. & S. Zhang (1990) Finite element interpolation of nonsmooth functions satisfying boundary conditions. *Math. Comp.*, **54**, 483–493.
Wong, S. H. & Z. J. Cendes (1988) Combined finite element-modal solution of three-dimensional eddy current problems. *IEEE Trans. Magnet.*, **24**, 2685–2687.
Zhang, S. (2005) A new family of stable mixed finite elements for the 3D Stokes equations. *Math. Comp.*, **74**, 543–54.

Appendix A. Proof of Lemma 3.1

In order to describe the new interpolant we first remind the reader of the Scott–Zhang interpolant (Scott & Zhang, 1990). For every $z \in \mathcal{V}_h$ we define $\phi_z \in \mathcal{P}_1^c(\mathcal{T}_h)$ to be the hat function $\phi_z(y) = \delta_{yz}$ for all $y \in \mathcal{V}_h$. Also for every $z \in \mathcal{V}_h$ we identify an arbitrary edge e_z of the mesh that contains z with the only constraint that e_z is a boundary edge if z is a boundary vertex. Then there exists a function $\psi_z \in L^\infty(e_z)$ such that

$$\int_{e_z} \psi_z \phi_y = \delta_{yz}, \qquad y \in \mathcal{V}_h. \tag{A.1}$$

Moreover,

$$\|\psi_z\|_{L^\infty(e_z)} \leqslant \frac{C}{|e_z|}. \tag{A.2}$$

The Scott–Zhang interpolant $\tilde{\boldsymbol{I}}_h$, acting on $\boldsymbol{\tau} \in \boldsymbol{H}^{\frac{1}{2}+\delta}(\Omega)$, is given by

$$\tilde{\boldsymbol{I}}_h \boldsymbol{\tau}(x) = \sum_{z \in \mathcal{V}_h} \left(\int_{e_z} \psi_z \boldsymbol{\tau} \right) \phi_z(x). \tag{A.3}$$

Although the Scott–Zhang interpolant has the approximation properties we need, it might not preserve the tangential trace to be zero. More precisely, if $\boldsymbol{\tau} \in \boldsymbol{H}^{\frac{1}{2}+\delta}(\Omega) \cap \boldsymbol{H}_0(\mathrm{rot}; \Omega)$, then $\tilde{\boldsymbol{I}}_h \boldsymbol{\tau} \cdot \boldsymbol{t}$ might not vanish on edges that touch a corner vertex. Therefore, we must modify the Scott–Zhang interpolant on such vertices.

For every corner boundary vertex $z \in \mathcal{V}_h^C$ we will consider the two boundary edges, e_z^1, e_z^2, which have z as an endpoint. We let $\boldsymbol{n}_z^i$ be the outward-pointing normal to e_z^i and $\boldsymbol{t}_z^i$ the tangent vector to $\boldsymbol{n}_z^i$ that is rotated 90 degrees counterclockwise. We then have the existence of $\psi_z^i \in L^\infty(e_z^i)$ such that

$$\int_{e_z^i} \psi_z^i \phi_y = \delta_{yz}, \qquad y \in \mathcal{V}_h, \tag{A.4}$$

$$\|\psi_z^i\|_{L^\infty(e_z^i)} \leqslant \frac{C}{|e_z|}. \tag{A.5}$$

We can then define the modified Scott–Zhang interpolant as

$$\boldsymbol{I}_h \boldsymbol{\tau}(x) := \sum_{z \in \mathcal{V}_h \setminus \mathcal{V}_h^C} \left(\int_{e_z} \psi_z \boldsymbol{\tau} \right) \phi_z(x) + \sum_{z \in \mathcal{V}_h^C} \boldsymbol{\beta}_z(\boldsymbol{\tau}) \phi_z(x), \tag{A.6}$$

where

$$\boldsymbol{\beta}_z(\boldsymbol{\tau}) := \frac{\boldsymbol{n}_z^2}{\boldsymbol{n}_z^2 \cdot \boldsymbol{t}_z^1} \int_{e_z^1} (\boldsymbol{\tau} \cdot \boldsymbol{t}_z^1)\psi_z^1 + \frac{\boldsymbol{n}_z^1}{\boldsymbol{n}_z^1 \cdot \boldsymbol{t}_z^2} \int_{e_z^2} (\boldsymbol{\tau} \cdot \boldsymbol{t}_z^2)\psi_z^2.$$

We now proceed to prove Lemma 3.1 in four steps.

(i) $\boldsymbol{I}_h : \boldsymbol{H}^{\frac{1}{2}+\delta}(\Omega) \cap \boldsymbol{H}_0(rot;\Omega) \to \mathbf{P}_1^c(\mathcal{T}_h) \cap \boldsymbol{H}_0(rot,\Omega)$: If $\boldsymbol{\tau} \in \boldsymbol{H}^{\frac{1}{2}+\delta}(\Omega) \cap \boldsymbol{H}_0(\mathrm{rot};\Omega)$, then clearly $\boldsymbol{I}_h\boldsymbol{\tau}(z) = 0$ for every $z \in \mathcal{V}_h^C$. Also we have $\boldsymbol{I}_h\boldsymbol{\tau}(z) \cdot \boldsymbol{t}_z = 0$ for all $z \in \mathcal{V}_h \backslash \mathcal{V}_h^C$ where $\boldsymbol{t}_z$ is tangent to e_z. Thus we have that $\boldsymbol{I}_h\boldsymbol{\tau} \cdot \boldsymbol{t} = 0$ on $\partial\Omega$.

(ii) $\boldsymbol{I}_h$ *is a projection*: In order to show it is a projection we need to show that $\boldsymbol{I}_h\boldsymbol{\tau}(z) = \boldsymbol{\tau}(z)$ for all $z \in \mathcal{V}_h$ and $\boldsymbol{\tau} \in \mathbf{P}_1^c(\mathcal{T}_h)$. To this end let $\boldsymbol{\tau} \in \mathbf{P}_1^c(\mathcal{T}_h)$. If $z \in \mathcal{V}_h \backslash \mathcal{V}_h^C$ then $\boldsymbol{I}_h\boldsymbol{\tau}(z) = \int_{e_z} \psi_z\boldsymbol{\tau}$. However, $\int_{e_z} \psi_z\boldsymbol{\tau} = \boldsymbol{\tau}(z)$ by (A.1), since $\boldsymbol{\tau}|_{e_z} = \boldsymbol{\tau}(z)\phi_z + \boldsymbol{\tau}(y)\phi_y$ where y is the other endpoint of e_z. On the other hand, if $z \in \mathcal{V}_h^C$ then $\boldsymbol{I}_h\boldsymbol{\tau}(z) = \boldsymbol{\beta}_z(\boldsymbol{\tau})$. Then we have $\boldsymbol{\beta}_z(\boldsymbol{\tau}) \cdot \boldsymbol{t}_z^i = \int_{e_z^i} (\boldsymbol{\tau} \cdot \boldsymbol{t}_z^i)\psi_z^i$. Using (A.1) we have $\int_{e_z^i} (\boldsymbol{\tau} \cdot \boldsymbol{t}_z^i)\psi_z^i = \boldsymbol{\tau}(z) \cdot \boldsymbol{t}_z^i$. Thus we have shown that $\boldsymbol{I}_h\boldsymbol{\tau}(z) \cdot \boldsymbol{t}_z^i = \boldsymbol{\tau}(z) \cdot \boldsymbol{t}_z^i$ for $i = 1, 2$ and thus $\boldsymbol{I}_h\boldsymbol{\tau}(z) = \boldsymbol{\tau}(z)$.

(iii) Stability estimate: We derive a stability estimate following the arguments of Ciarlet (2013), Scott & Zhang (1990). First we note that by an inverse estimate we have

$$|\boldsymbol{I}_h\boldsymbol{\tau}|_{H^{\frac{1}{2}+\delta}(T)} \leqslant Ch_T^{-\frac{1}{2}-\delta} \|\boldsymbol{I}_h\boldsymbol{\tau}\|_{L^2(T)}.$$

Thus, we only need to bound the L^2 norm. To do this we first note the trace inequality (cf. Ciarlet, 2013, Proposition 3.1)

$$\|\boldsymbol{\tau}\|_{L^1(e_z)} \leqslant C\big(\|\boldsymbol{\tau}\|_{L^2(T)} + h_T^{\frac{1}{2}+\delta} |\boldsymbol{\tau}|_{H^{\frac{1}{2}+\delta}(T)}\big),$$

for $T \in \mathcal{T}_h$ with $e_z \subset \partial T$. We remind the reader that the number of corner points $\mathcal{V}_h^C$ is finite and independent of the mesh $\mathcal{T}_h$ and hence $M := \max_{z \in \mathcal{V}_h^C} \frac{1}{|\boldsymbol{n}_z^1 \cdot \boldsymbol{t}_z^2|}$ is finite. Thus, using (A.2) and (A.5), we have

$$\begin{aligned}
\|\boldsymbol{I}_h\boldsymbol{\tau}\|_{L^2(T)} &\leqslant \sum_{\substack{z \in \mathcal{V}_h \backslash \mathcal{V}_h^C \\ z \in \bar{T}}} \|\phi_z\|_{L^2(T)} \|\psi_z\|_{L^\infty(e_z)} \|\boldsymbol{\tau}\|_{L^1(e_z)} \\
&\quad + M \sum_{\substack{z \in \mathcal{V}_h^C \\ z \in \bar{T}}} \|\phi_z\|_{L^2(T)} \big(\|\psi_z^1\|_{L^\infty(e_z^1)} \|\boldsymbol{\tau}\|_{L^1(e_z^1)} + \|\psi_z^2\|_{L^\infty(e_z^2)} \|\boldsymbol{\tau}\|_{L^1(e_z^2)}\big) \\
&\leqslant C(1+M)\big(\|\boldsymbol{\tau}\|_{L^2(\omega(T))} + h_T^{\frac{1}{2}+\delta} |\boldsymbol{\tau}|_{H^{\frac{1}{2}+\delta}(\omega(T))}\big),
\end{aligned}$$

where we used that $\|\phi_z\|_{L^2(T)} \leqslant Ch_T$. Hence, combining the above results we obtain

$$h_T^{\frac{1}{2}+\delta} |\boldsymbol{I}_h\boldsymbol{\tau}|_{H^{\frac{1}{2}+\delta}(T)} + \|\boldsymbol{I}_h\boldsymbol{\tau}\|_{L^2(T)} \leqslant C(1+M)\big(\|\boldsymbol{\tau}\|_{L^2(\omega(T))} + h_T^{\frac{1}{2}+\delta} |\boldsymbol{\tau}|_{H^{\frac{1}{2}+\delta}(\omega(T))}\big). \tag{A.7}$$

(iv) Estimate (3.1): Let $\boldsymbol{w} = \frac{1}{|\omega(T)|} \int_{\omega(T)} \boldsymbol{\tau}$; we have

$$\|\boldsymbol{\tau} - \boldsymbol{w}\|_{L^2(\omega(T))} \leqslant Ch_T^{\frac{1}{2}+\delta} |\boldsymbol{\tau}|_{H^{\frac{1}{2}+\delta}(\omega(T))}. \tag{A.8}$$

Estimate (A.8) for $\delta = \frac{1}{2}$ is shown in Scott & Zhang (1990, Section 4). Estimate (A.8) for $\delta \in (0, \frac{1}{2})$ can be found for example in Drelichman & Durán (2018, Proposition 2.1) and Bellido & Mora-Corral (2014, Lemma 3.1). See also Ern & Guermond (2017, Lemma 5.6).

Because $\boldsymbol{w}$ is constant we have that $\boldsymbol{I}_h \boldsymbol{w} = \boldsymbol{w}$ on T, and thus using (A.7) and (A.8) we obtain

$$\begin{aligned}\|\boldsymbol{I}_h\boldsymbol{\tau} - \boldsymbol{\tau}\|_{L^2(T)} &= \|\boldsymbol{I}_h(\boldsymbol{\tau} - \boldsymbol{w}) + (\boldsymbol{w} - \boldsymbol{\tau})\|_{L^2(T)} \\ &\leqslant C(1+M)\big(\|\boldsymbol{\tau} - \boldsymbol{w}\|_{L^2(\omega(T))} + h_T^{\frac{1}{2}+\delta}|\boldsymbol{\tau}|_{H^{\frac{1}{2}+\delta}(\omega(T))}\big) \\ &\leqslant C(1+M)\big(h_T^{\frac{1}{2}+\delta}|\boldsymbol{\tau}|_{H^{\frac{1}{2}+\delta}(\omega(T))}\big).\end{aligned}$$

Similarly, $|\boldsymbol{I}_h\boldsymbol{\tau}|_{H^{\frac{1}{2}+\delta}(T)} = |\boldsymbol{I}_h\boldsymbol{\tau} - \boldsymbol{w}|_{H^{\frac{1}{2}+\delta}(T)} = |\boldsymbol{I}_h(\boldsymbol{\tau} - \boldsymbol{w})|_{H^{\frac{1}{2}+\delta}(T)}$ and one can use (A.7) and (A.8) again to get $|\boldsymbol{I}_h\boldsymbol{\tau}|_{H^{\frac{1}{2}+\delta}(T)} \leqslant C(1+M)|\boldsymbol{\tau}|_{H^{1/2+\delta}(\omega(T))}$. This completes the proof of Lemma 3.1.